
Chapter 3

Results and Discussion

3.1 Domain architecture of the human AF6 Protein

The human AF6 protein contains two N-terminal Ras-association (RA) domains one forkhead association (FA) domain, one class V myosin homology domain (dilute domain, DIL) and a postsynaptic density/Discs large/zona occludens-1 (PDZ) domain. (Figure 3.1) The PDZ domain of AF6 mediates the interaction with a subset of ephrine receptor protein-tyrosine kinases,^{1,2} the poliovirus receptor-related protein PRR2/nectin,³ the junctional adhesion molecule (JAM)⁴ and the breakpoint cluster region protein (BCR)⁵. In this chapter, we describe the discovery of small, non-covalent ligands for the AF6 PDZ domain by NMR based screening methods, and their subsequent modification to improve affinity. In the second half of the chapter, structure determination of the AF6 PDZ and AF6 PDZ domain in complex with an organic compound is described.

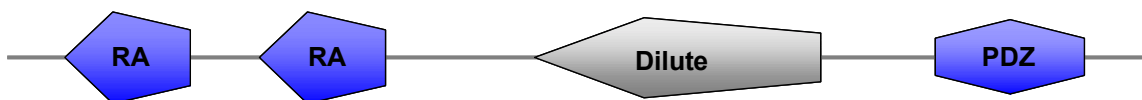


Figure 3.1: Domain architecture of the AF6 Protein. Domains and the domain boundaries were identified from the PROSITE database.

3.2 Expression and purification of the recombinant AF6 PDZ domain

For over-expression of the AF6 PDZ domain a pGEX-6P-2 vector containing the AF6 PDZ domain as a C-terminal fusion protein of glutathione-S-transferase (GST) was used. Over-expression of the fusion protein was carried out in *E.coli* strain BL21-DE3. Figure 3.2 shows the amino acid sequence of the AF6 PDZ domain.

For screening purposes U-¹⁵N labeled AF6 PDZ domain was obtained by growing the cells in a media containing ¹⁵NH₄Cl as a sole source of nitrogen. The

fusion protein was purified by affinity chromatography on a glutathione column, cleaved using PreScission protease, and the PDZ domain was obtained in purified form after gel filtration chromatography. Optimization of the cell growth and induction conditions led to the final yields of 40 mg per liter of AF6 PDZ domain. Figure 3.3 shows the progress of the purification procedure. The resulting samples were checked by SDS-PAGE and Mass Spectrometry for purity and by ^1H - ^{15}N HSQC experiments for stability.

For structure determination U- ^{13}C and ^{15}N labeled samples were purified by using ^{13}C -glucose and $^{15}\text{NH}_4\text{Cl}$ as sole carbon and nitrogen sources, respectively. Mass spectrometry analysis confirmed that isotopically enriched protein was produced.

1 11 21 31 41

GPLGSLRKEP EIITVTLKKQ N **GMGL** SIVAA KGAGQDKLG IYVKS~~V~~VKGGGA

51 61 71 81 91

ADV~~D~~GR~~L~~LAAG DQLLSVDGRS LVGLSQERAA ELMTRTSSV~~V~~ TLEVAKQGA~~I~~Y

Figure 3.2: Amino acid sequence of the AF6 PDZ domain. The conserved “GLGF” loop of the PDZ domains (replaced by “GMGL” in the AF6 PDZ domain) is highlighted in magenta.

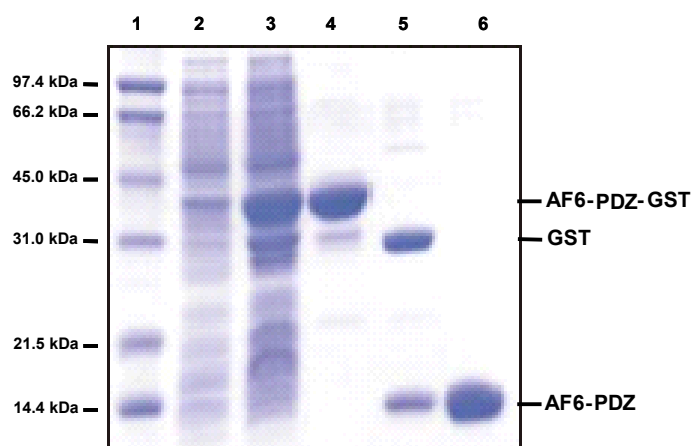


Figure 3.3: Expression of AF6 PDZ domain in M9 minimal media. Lane 1: Markers; Lane 2: Before induction; Lane 3: After induction with IPTG; Lane 4: After affinity chromatography on GST-Sepharose column; Lane 5: PreScission peotase cleavage; Lane 6: After gelfiltration chromatography.

3.3 NMR based screening of ligands for the AF6 PDZ domain

AF6 PDZ domain adopts a stable fold in solution and is known to interact with its natural peptide ligands according to the canonical PDZ binding mode.⁶ Prior to this study non-covalent, synthetic small molecule ligands to PDZ domains were not known. Therefore to identify novel, non-covalent, small molecule ligands for the AF6 PDZ domain we used ¹H-¹⁵N HSQC NMR-based screening technique because of its high sensitivity towards weakly binding ligands, coupled with its unique ability to provide structural support for fragment based lead optimization. Using the AF6 PDZ domain as representative model, 5,000 compounds from the ~20,000 FMP compound library were screened for their activity against the AF6 PDZ domain. The library consists of low molecular weight compounds specifically chosen for NMR based screening. It was designed according to the Lipinski Rule of 5⁷ which predicts poor absorption or permeation is more likely when there are more than 5 hydrogen bond (H-bond) donors, 10 H-bond acceptors, the molecular weight is greater than 500 and the calculated Log P (CLogP) is greater than 5. Also, the library has representative abundance of functional groups and scaffolds frequently occurring in approved drugs.^{8,9} All compounds were initially tested for their solubility under typical assay conditions (500 μM ligand in phosphate buffer; pH 6.5, 10% d₆-DMSO).

3.3.1 Screening results

As the ¹H-¹⁵N HSQC based screening experiments are relatively time consuming and require uniformly ¹⁵N labeled samples at high concentrations, it is not possible to screen large compound libraries by this method. In order to save time and reduce sample consumption, a representative library of 5,000 compounds from the FMP compound collection was screened against the AF6 PDZ domain. This representative library samples most of the functional groups in the 20,000 compounds library. From an analysis of the pattern of chemical shift changes for the hits, three chemically distinct classes of compounds binding to the AF6 PDZ domain were identified. Comparing the structures of the compounds to the conserved C-terminal valine of natural peptide ligands (Figure 3.4) reveals a consistent pharmacophore pattern of one moiety showing at least one hydrogen

bond acceptor (green), a moiety showing one hydrogen bond donor (blue), and a hydrophobic core of variable size. Compound **3** occurs in two tautomeric forms in aqueous solution and in organic solvents. For compound **3** this H bond donor/acceptor similarity is achieved for only one out of three feasible tautomeric forms.

The positive hits from the screening were found to bind to the same site on the AF6 PDZ domain, as evidenced by the similar pattern of chemical shift perturbations (CSPs) (Table 3.1). More importantly, the compounds were found to bind in or near the peptide binding groove as shown in figure 3.5. To derive comprehensive structure-activity relationships (SAR), several commercially available analogues of the hits were purchased and evaluated for their binding activity.

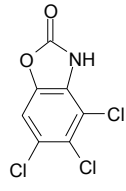
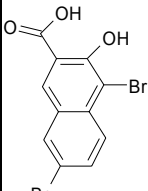
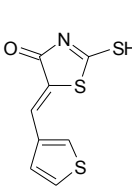
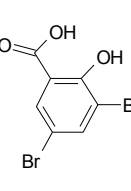
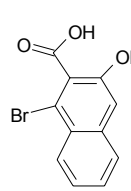
					
IQSVEV _{COOH}	1	2	3	4	5
G24					G22
L25	L 25		L 25	L25	
S26	S 26		S 26	S 26	S 26
I27		I 27	I 27	I27	I 27
V28		V 28			V 28
	A29				
		A30			A30
		V42			
		K 43			K 43
		S44			S 44
V46		V 46	V 46	V46	V 46
S48					
		A50	A50		
	A51		A51	A51	
G60		G 60			G 60
		Q62	Q62	Q62	
A80		A80			
					E81
L82	L82		L 82	L82	L 82
	M 83	M 83	M 83	M 83	M 83
T84	T 84	T 84	T 84	T 84	T 84
	R 85	R 85	R85	R 85	R 85
					T86
S88					
V90		V 90			V90
T91		T91			

Table 3.1: “Hits” identified for the AF6 PDZ domain by NMR based screening. Residues with strong chemical shifts ($\delta\Delta > 0.3$ ppm) are highlighted in red while the residues with moderate chemical shift change ($\delta\Delta > 0.1 > 0.3$ ppm) are highlighted in yellow.

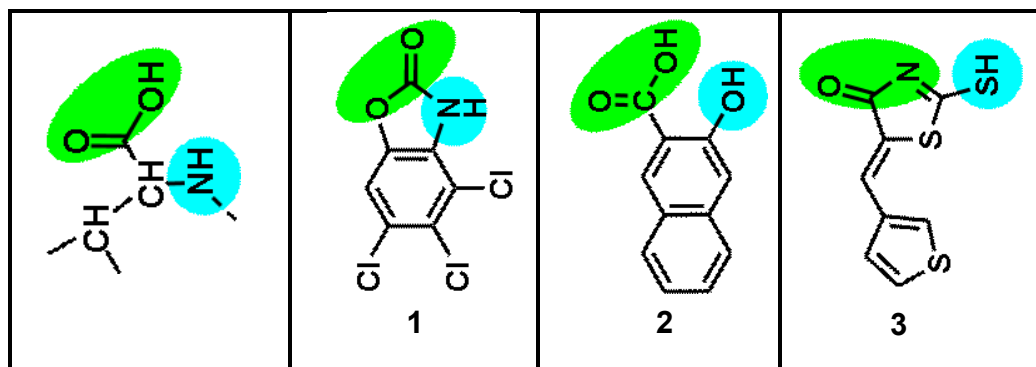


Figure 3.4: General hit scaffold identified for the AF6 PDZ domain. Hydrogen bond acceptors are highlighted in green and hydrogen bond donors are highlighted in blue.

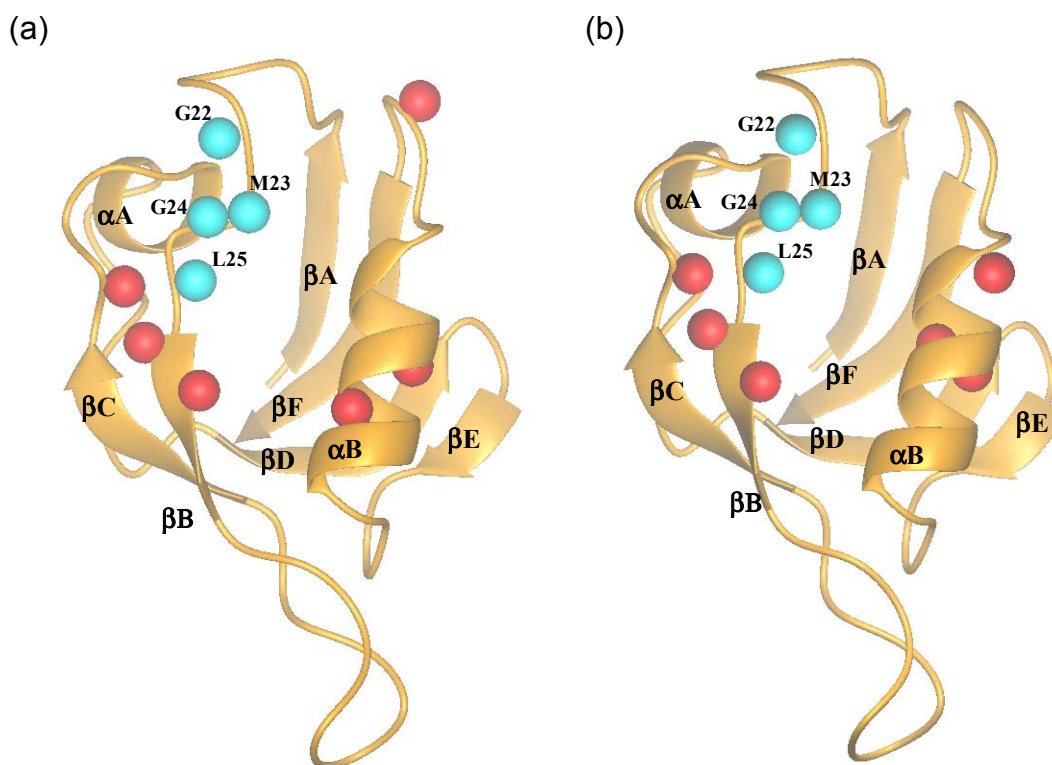


Figure 3.5: Exemplary CSPs and binding sites of screening hits. Strongly shifting backbone HN's are shown as red spheres. The backbone HN's of the residues in the GMGL loop are shown as blue spheres. a) Peptide ligand (IQSVEV) b) Compound 3

Dissociation constants were derived for the positive hits which exhibited the strongest CSPs by monitoring the protein HN chemical shift change as a function of the ligand concentration and are listed in Table 3.2.

Compound No	Binding constant (μM)
1	680 ± 33
2	635 ± 28
3	460 ± 32
4	> 1000
5	> 1000

Table 3.2: Apparent dissociation binding constants (K_d) as derived from NMR titration experiments for the most active compounds listed in table 3.1.

Taking into account the highest activity of **3** and the feasibility to generate a focused library of the analogues using simple chemical procedures, it was chosen for further work. The synthesis and purification of the compounds was done by Ms. Carolyn Vargas (FMP, Berlin). Activity of the compounds in the library to the present date is given in table 3.3.

As shown in the table 3.3, thienyl (**6a**), furanly (**6b**) and phenyl (**6c**) substituents at the R^1 position showed weak binding activity towards the AF6 PDZ domain as judged by the CSPs. In contrast, the *meta* and the *para* methyl substitution of the phenyl ring (**6d** and **6e**, respectively) render the compounds inactive. The analogues with an isopropyl (**6f**) substituent at R^1 showed weak activity towards the protein. Bromine or a trifluoromethyl substituent at the *p*-position (**6h** and **6i** respectively) of the phenyl ring exhibited binding affinity. Also, the compounds having *meta* trifluoromethyl or *meta* bromo substituted phenyl rings were found to interact with the AF6 PDZ domain (**6j** and **6k** respectively).

A significant improvement in the binding was observed for the 5-aryl-2-thioxo-4-thiazolidinone analogues (**7a** to **7i**). The compound with the *para* substituted trifluoromethyl group (**7i**) exhibited the strongest binding of all investigated compounds. However, the analogue with *m*-trifluoromethyl substituted phenyl ring (**7k**) exhibited weak activity.

From the obtained results it is evident that the phenyl ring in the R¹ position of **6** and **7** is important for the activity. Also the strength of the interaction is governed by the position of the substituent on the aforementioned phenyl ring. Secondly, analysis of analogous compounds having 2-oxo-4-thiazolidinone head group (Table 3.4) showed comparatively lower activity than their 2-thioxo-4-thiazolidinone counterparts implying that the 2-thioxo group in the head group plays some role in the protein-ligand interaction.

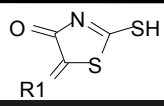
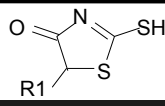
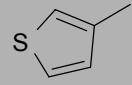
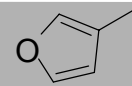
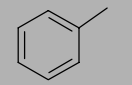
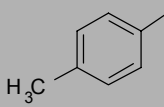
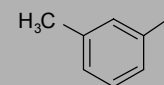
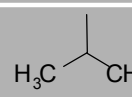
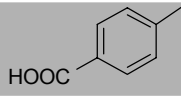
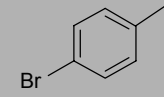
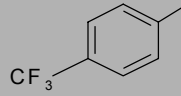
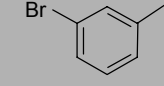
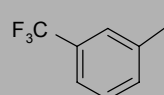
			
	R1	Activity	Activity
a		++	++
b		+	++
c		++	+
d		-	ND
e		-	-
f		+	+
g		-	ND
h		+++	+++
i		++	+++
j		-	ND
k		+	-

Table 3.3: Relative activity of 2-thioxo-4-thiazolidinone analogs. i) +, ++, and +++ indicate more than 3 residues showing chemical shift changes ($\Delta\delta$) in the range $0.1 \leq \Delta\delta \leq 0.3$, $0.3 \leq \Delta\delta \leq 0.5$, and $\Delta\delta > 0.5$, respectively. ii) Analyzed as racemate.

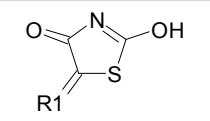
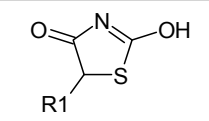
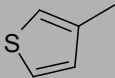
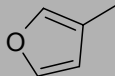
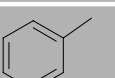
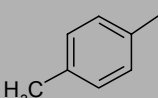
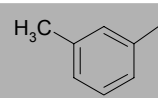
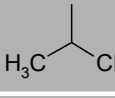
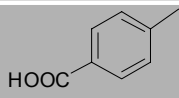
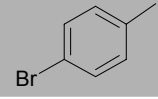
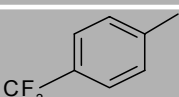
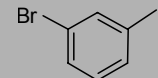
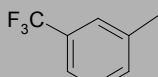
			
	R1	Activity	Activity
a		+	-
b		+	-
c		-	-
d		-	-
e		-	-
f		+	ND
g		-	ND
h		-	ND
i		-	+
j		+	-
k		+	++

Table 3.4: Relative activity of 2-oxo-4-thiazolidinone analogs. i) +, ++, and +++ indicate more than 3 residues showing chemical shift changes ($\Delta\delta$) in the range $0.1 \leq \Delta\delta \leq 0.3$, $0.3 \leq \Delta\delta \leq 0.5$, and $\Delta\delta > 0.5$, respectively. ii) Analyzed as racemate.

3.3.2 Dissociation constant and CSP map of 5-(4-trifluoromethylbenzyl)-2-thioxo-4-thiazolidinone (**7i**)

Based on the NMR derived binding constants, **7i** was found to be the most active compound and was hence chosen for further structural studies. For dissociation constant determination a series of ^1H - ^{15}N HSQC spectra were determined at various **7i** concentrations. Figure 3.6a shows the chemical shift difference for selected residues as a function of **7i** concentration. The data were fit using one-site binding model. By this method a dissociation constant of 100 μM was calculated for **7i**. Racemic mixture of the ligand was used in the measurements. Assuming that only one of the enantiomer binds preferentially, the affinity of the compound can be approximated to 50 μM which is in the same range as that of the natural peptide ligands.

Figure 3.6b shows the CSP map of **7i**. As seen the figure largest CSPs are observed for the residues around the peptide binding groove of the AF6 PDZ domain (residues in the βB and αB), therefore it can be safely assumed that **7i** binds to the AF6 PDZ domain in the vicinity of the peptide binding groove.

3.3.3 5-(4-trifluoromethylbenzyl)-2-thioxo-4-thiazolidinone (**7i**) interacts competitively with the AF6 PDZ domain

To demonstrate that **7i** binds competitively to the AF6 PDZ domain, a series of ^{15}N -filtered ^1H spectra with increasing amount of the test compound (**7i**) were recorded on a sample containing equimolar concentrations of U- ^{15}N labeled AF6 PDZ and a known binder ($_{\text{NH}_2}\text{-IQSVEV-COOH}$). As shown in figure 3.7, the peptide signal at 8.07 ppm, which vanishes in the presence of the protein, reemerges as a function of **7i** concentration. Also the signal at 8.3 ppm reverts back to the “unbound” state. The other signals of the peptide were unobservable because of the overlap between the signals of the peptide and the aromatic protons of **7i**.

To check the authenticity of the competitive binding study, control experiments were performed by adding equivalent amounts of $\text{d}_6\text{-DMSO}$ to a equimolar solution of $_{\text{NH}_2}\text{-IQSVEV-COOH}$ and AF6 PDZ domain. No significant changes to the

above mentioned peptide signals at 8.07 and 8.3 ppm were observed. Also the stability of the protein under the experimental conditions was confirmed by recording ^1H - ^{15}N HSQC spectra at the beginning and end of the titration. These control experiments underscore that the aforementioned signal reemergence is due to the displacement of peptide ligand from the proteins binding groove in presence of **7i**.

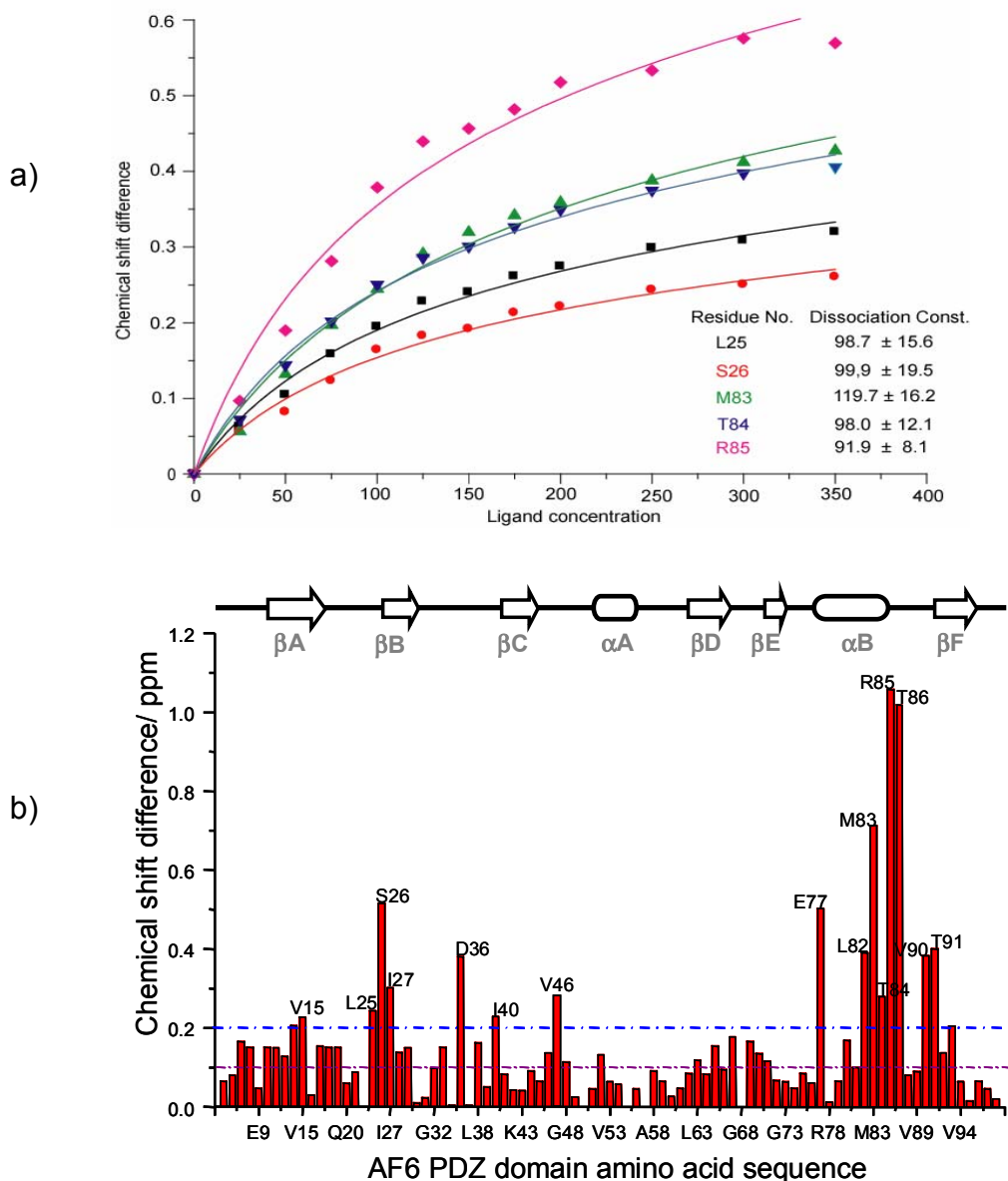


Figure 3.6: a) Binding constant determination for **7i**. The data were fitted by assuming a single site binding model. b) CSPs in the backbone HN's of the AF6 PDZ in the presence of **7i**.

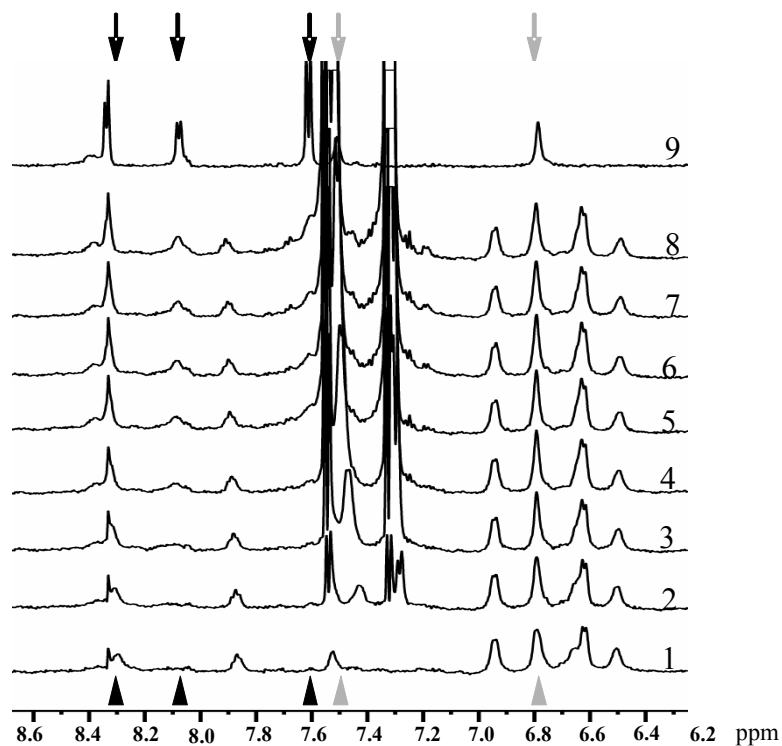


Figure 3.7: Competition binding experiment. Stack plots of the ¹⁵N-Filtered 1D Watergate experiments are shown. 1-8) Spectra recorded on a sample containing 100 μM U-¹⁵N labeled AF6 PDZ domain with 100 μM IQSVEV peptide, the spectra were recorded at 0, 100, 200, 400, 600, 800, 1000 and 1400 μM 7i respectively. 9). Spectrum of IQSVEV alone under experimental conditions.

3.4 Structure determination of the AF6 PDZ domain and AF6 PDZ - 5-(4-trifluoromethylbenzyl)-2-thioxo-4-thiazolidinone (**7i**) complex

3.4.1 Resonance assignments

Small proteins (<10 kDa) can be easily assigned by using traditional experiments like NOESY, COSY and TOCSY. But this approach suffers heavily from the multiple assignment possibilities in the recorded spectra. A much better approach is to use resonances assignments methods based on the triple resonance experiments. This approach is very well suited for assigning moderately sized proteins (< 20 kDa). For the AF6 PDZ domain and AF6 PDZ in complex with the peptide and organic ligand fast and reliable chemical shift assignments were done by triple resonance correlation experiments. Multiple pairs of these correlation experiments were used for removing the ambiguity or loss of information from one set of experiment. All spectra were assigned using the software SPARKY.¹⁰

3.4.1.1 Backbone chemical shift chemical shift assignment

Backbone chemical shift assignments for the AF6 PDZ domain are described earlier.⁶ Sequence specific backbone ¹HN, ¹⁵N and ¹³C chemical shift assignments of the AF6 PDZ domain in complex with **7i** were obtained using the CBCA(CO)NH and CBCANH experiment pair.

Figure 3.8 shows the ¹H-¹⁵N HSQC spectra for the AF6 PDZ domain in complex with **7i** (1:1 protein ligand ratio). The resonances are well resolved and indicate a folded protein.

Nearly complete backbone chemical shift assignments were obtained using the triple resonance experiments. Characteristic downfield C β chemical shifts of threonine and serine residues and the upfield chemical shifts of the alanine C β 's served as the starting points for the assignments (Figure 3.9). By walking along the protein backbone, almost complete assignment for the C α , C β , N and HN spins was achieved using the CBCA pair of triple resonance experiments.

HBHA(CO)NH and HBHANH pair of experiments were used for the assignments of the H α and H β spins.

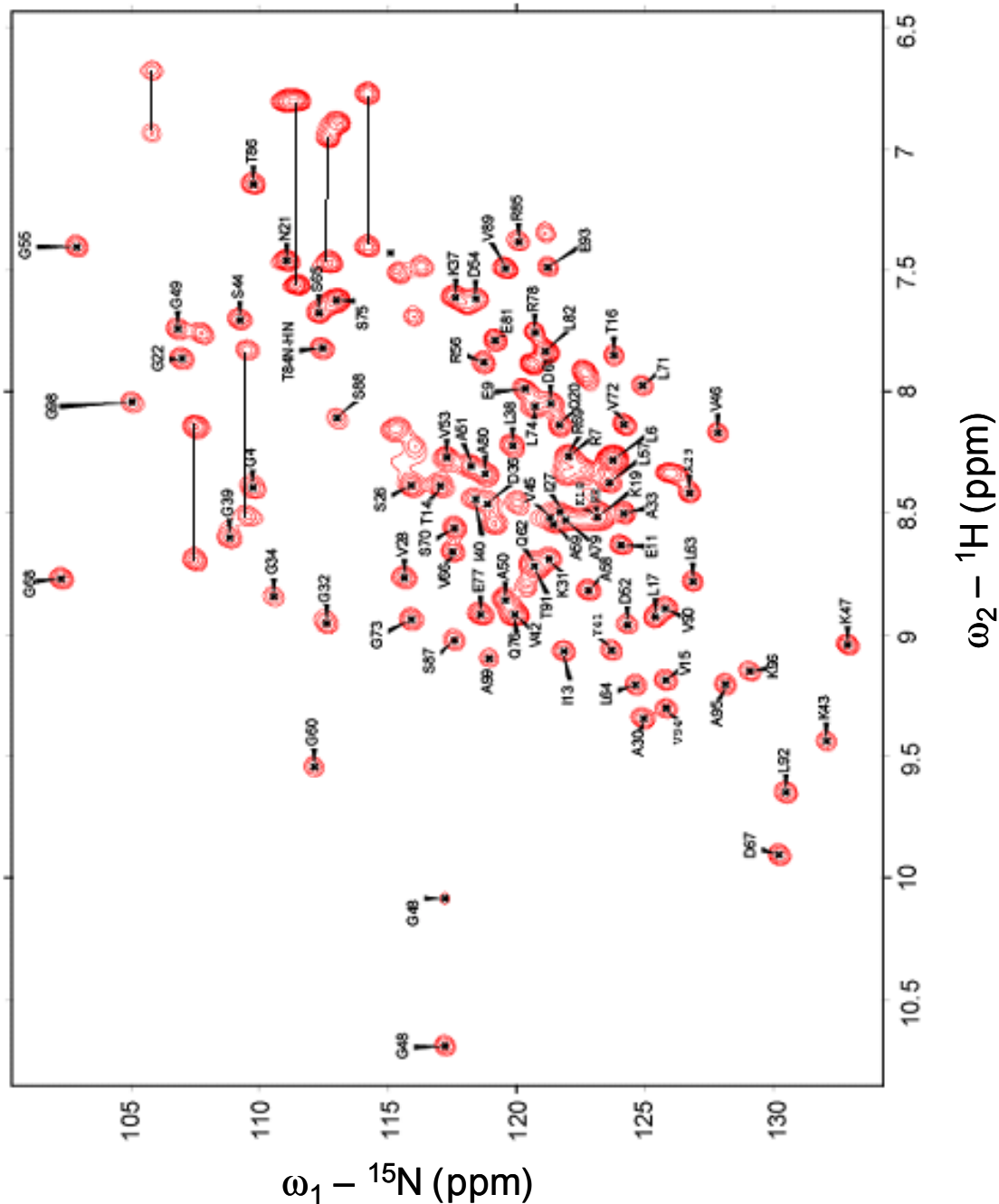


Figure 3.8: ^1H - ^{15}N HSQC spectrum of the AF6 PDZ domain in presence of **7i** recorded at 300 K on a Bruker DRX 600 spectrometer. The spectrum was recorded on 1:1 mixture of AF6 PDZ and **7i** at 1.5mM concentration.

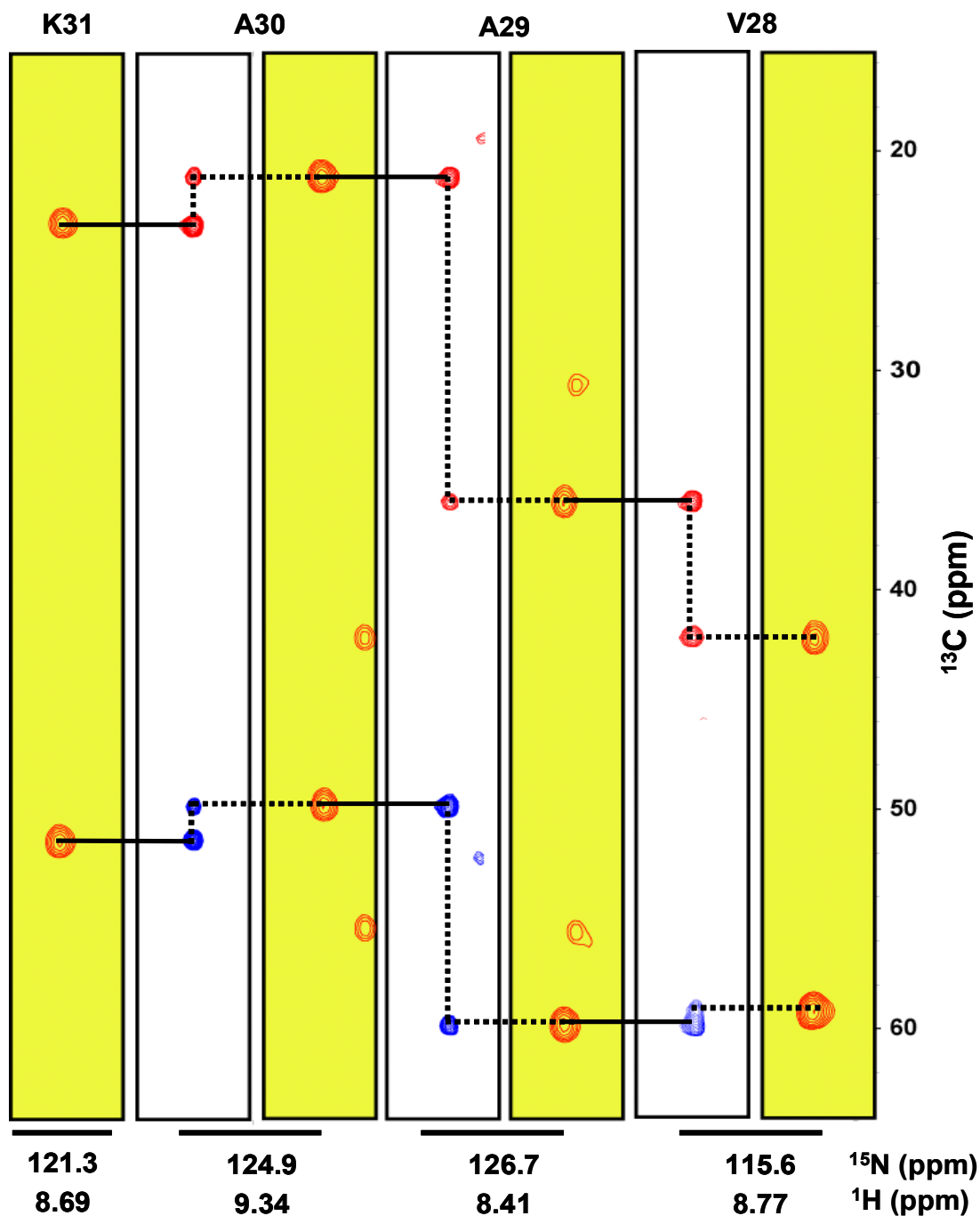


Figure 3.9: Strip plots of the CBCA(CO)NH (yellow background) and CBCANH (white background) spectra. Sequential connectivities for the protein backbone were obtained by connecting the C α and C β signals of $i-1^{\text{th}}$ residue in the CBCACONH (Red peaks, positive phase) with the C α (Blue peaks, negative phase) and C β (Red peaks, positive phase) of the i and $i-1^{\text{th}}$ residue in the CBCANH experiments.

3.4.1.2 Side-chain ^1H and ^{13}C Resonance Assignments

3.4.1.2.1 Assignment of Aliphatic Side-chains

Following the backbone resonance assignments, it was then necessary to assign the ^1H and ^{13}C nuclei of the amino acid side-chains. Aliphatic side chain assignments for the AF6 PDZ domain was achieved using 3D HCCH-COSY and a 3D HCCH-TOCSY experiment. Assignment of the side chain was also aided by 3D H(CCCO)NH and 3D (H)CC(CO)NH experiments. The H(CCCO)NH correlates the ^{15}N and ^1HN resonances of residue i with the ^{13}C and ^1HC resonances of residue $i-1$ and the (H)CC(CO)NH experiment was used correlate the ^{15}N and ^1HN resonances of residue i with the ^{13}C resonances of residue $i-1$. Assignments for the majority of the side-chain ^{13}C and ^1H resonances were obtained from these experiments.

3.4.1.2.2 Assignment of Aromatic Side-chains

The above mentioned TOCSY type experiments could not be used for the assignment of aromatic side-chain resonances because the DIPSI-3 mixing sequence used for the TOCSY-transfer step does not encompass a sufficiently wide ^{13}C frequency range to allow isotropic mixing between aromatic and aliphatic ^{13}C nuclei. The assignments of the aromatic protons were therefore obtained using a 3D ^{13}C NOESY-HSQC experiment and a 2D ^{13}C -HMQC experiment.

The side chain assignments of the AF6 PDZ domain – **7i** complex were obtained in similar manner.

3.4.2 ^{15}N relaxation measurements

T_1 and T_2 relaxation times were measured for the individual residues of the AF6 PDZ domain and are shown in figure 3.10a and 3.10b. All the residues except 1-10 and 96-100 show similar patterns for the T_1 and T_2 relaxation rates. These results indicate that the AF6 PDZ domain folds with no internal mobility. The residues 1-10 and 96-100 are apparently unstructured. These results are consistent with the structures of other PDZ domains published in which the homologous residues towards the N and the C termini are also unstructured.

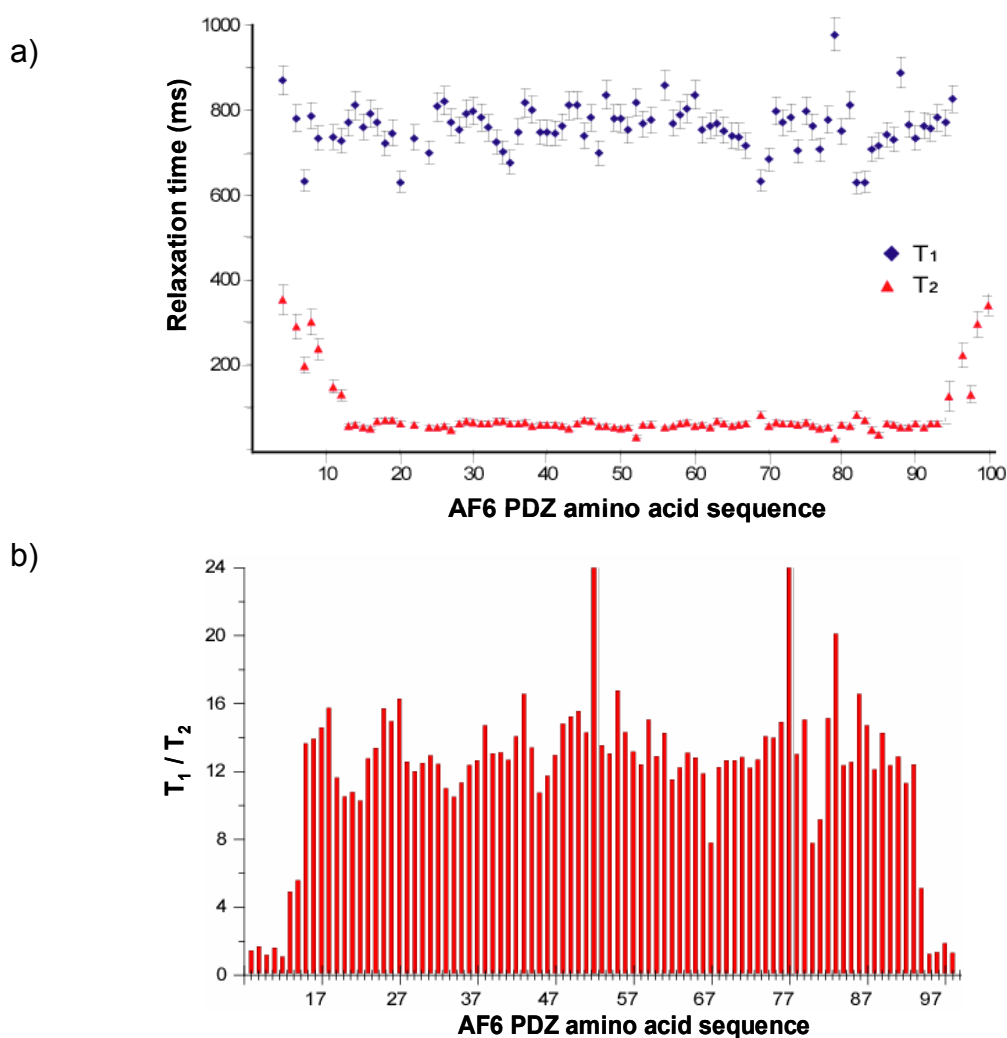


Figure 3.10: Relaxation properties of the backbone amides of AF6 PDZ domain. a) T_1 and T_2 relaxation rates of all the assigned residues. b) T_1/T_2 graph of the same residues.

3.4.3 Dihedral angle restraints

Based on the $C\alpha$, $C\beta$, N, NH, chemical shifts of all the assigned non-proline residues backbone ϕ and ψ torsional angles were predicted for the AF6 PDZ domain by using the program TALOS. Several values were predicted for each residue by TALOS and the predictions were checked visually based on the distribution of prediction in the Ramachandran plot. Only the angles which classified as “good” by the program were used in further calculation. All the torsional angles from TALOS were used in the calculations with an error margin of $\pm 20^\circ$.

3.4.4 Secondary structure prediction from the chemical shifts

Secondary structure of a protein under consideration can be predicted at an early stage in the structural investigation by NMR. Recently, methods that correlate backbone chemical shifts to secondary structural elements of the protein have been increasingly used for this purpose along with the more traditional NOE based and coupling constants based methods.^{11,12}

$C\alpha$, $C\beta$, C' and $H\alpha$ chemical shifts can be used to predict the secondary structure of the protein. Deviations in the chemical shifts of these atoms from those of the random coil can be used to identify the α -helical or extended regions of the protein. Consensus regions can be easily identified by assigning a chemical shift index (CSI) for each residue in the protein. A CSI of “1” indicates an increase in chemical shift of the residue with respect to the random coil, characteristic of a β -strand, while a CSI of “-1” indicates a decrease in chemical shift, characteristic of an α -helix. CSI value of “0” indicates no deviation from the random coil chemical shifts. An α -helix is identified by the presence of more than 4 uninterrupted “-1” CSI’s and a β -strand is identified by the presence of 3 or more “1” CSI’s.

Consensus CSI information of the AF6 PDZ domain and AF6 PDZ in complex with **7i** is shown in figure 3.11a and 3.11b respectively. For the AF6 PDZ domain the CSI plot clearly shows the presence of 4 β -strands (between residues 11-18,

25-31, 38-43 and 89-95) and 2 α -helices (residues 50-56 and 76-86). Although PDZ domains are known to have 6 β -strands, only 4 were predicted by the CSI and no overall consensus was obtained for the other two. For the AF6 PDZ in complex with **7i** the CSI was able to predict 5 β -strands. It is apparent that in the case of the AF6 PDZ domain the CSI can be reliably used for the prediction of the secondary structure stretches. It has to be taken into consideration that the start and finish of each secondary structure element is not definite and a NOE based model should be used to accurately define them. In summary the AF6 PDZ domains contains at least 5 β -strands: (residues 11-18, 25-31, 38-43, 62-67 and 89-95) and 2 α -helices (residues 50-56 and 76-86).

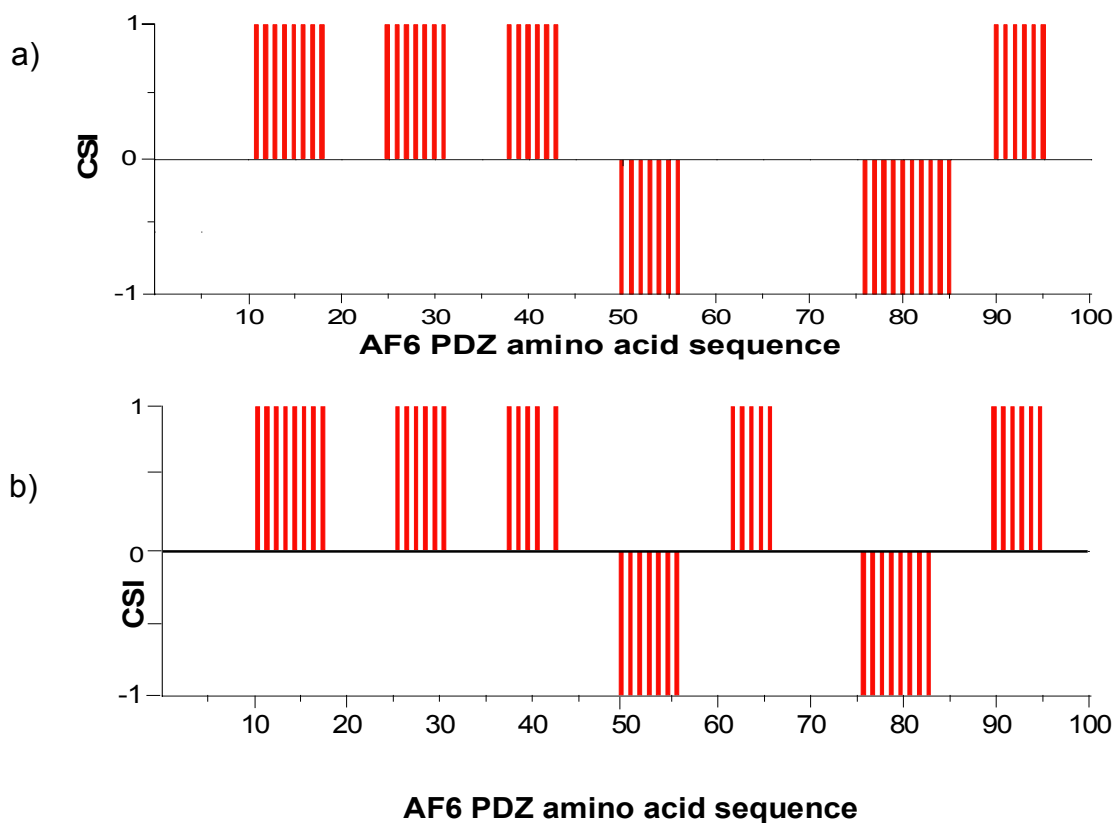


Figure 3.11: Consensus CSI plot for a) AF6 PDZ domain and b) AF6 PDZ domain in complex with **7i**. Scores were calculated from the supplied chemical shift lists using the program CSI (PENNY/MRC Group Joint Software Centre) are shown on the vertical axes.

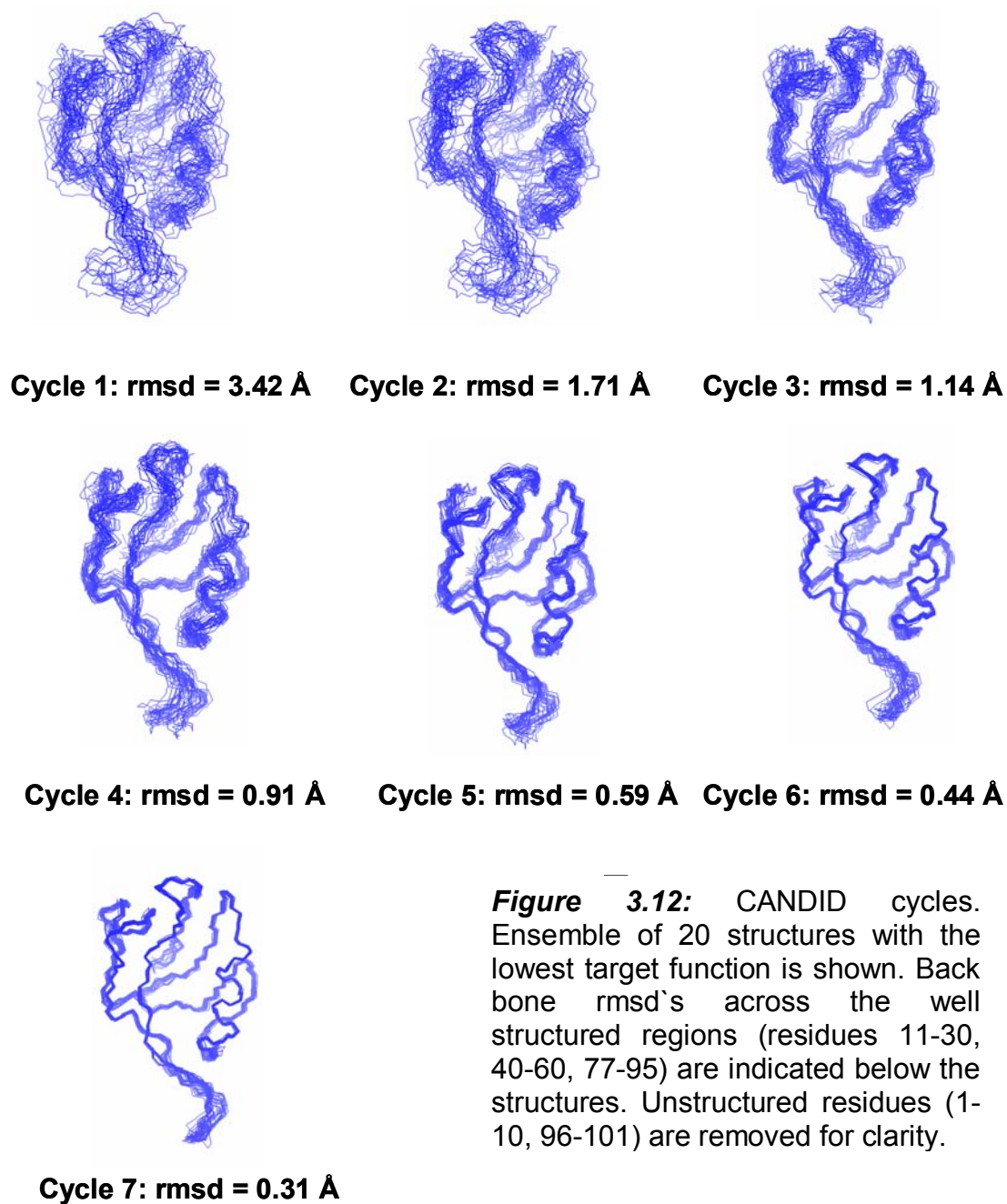
3.4.5 NOE assignments and structure calculation for the AF6 PDZ domain

The structures of the AF6 PDZ domain was determined by torsional angle dynamics using the CANDID (Combined Automated NOE assignment and structure Determination) module of the program CYANA. CANDID uses an iterative approach with multiple cycles of NOE assignment and structure calculation using the DYANA algorithm.¹³ The input for a CANDID cycle consists of the amino acid sequence, the NMR resonance list of the protein and the NOE peak list with the volume of each peak.

The procedure used by CANDID for structure calculation can be outlined as follows. Seven cycles of structure calculation and NOE assignments are performed automatically. The fold of the protein is established after the first cycle which relies heavily on the principle of network anchoring and constraint combination. The subsequent cycles contain the three dimensional structure information from the previous cycle. In the final cycle the assignments are filtered such that all accepted peaks have an unique assignment possibility. If this is not achieved the peak is left unassigned.

3.4.5.1 Application of CANDID for structure determination of the AF6 PDZ domain

The chemical shift assignments from section 3.4.1 and the corresponding NOE peak list with volumes were used as input for CANDID. In addition 60 torsional angle restraints from TALOS and 20 H-bonds were also used for structure determination. Chemical shift tolerances for the automated NOE assignments were kept at 0.02 ppm for the proton dimension and 0.3 ppm for the ¹³C/¹⁵N dimensions. Following manual inspection of the NOE assignments by CANDID, the final ensemble of structures was calculated using the restraints listed in table 3.5. Typically 200 structures were calculated by torsional angle dynamics (TAD) using a standard simulated annealing protocol. The 20 structures having the lowest target function value were accepted in the final ensemble during each cycle.



The convergence of individual structures starting from random coil is illustrated in figure 3.12.

The structural statistics of the final ensemble is listed in table 3.5. For the final structure calculation 1506 experimental restraints were used. CYANA identified 1426 distance restraints. Out of these 404 restraints were long-range distance restraints ($|i - j| > 4$) which define the global fold of the protein. Also, no distance

restraint violations $> 0.3 \text{ \AA}$ and no torsional angle restraint violations $> 5^\circ$ were observed.

Table 3.5: Structural statistics for the AF6 PDZ domain.

Restrains	
total no. of experimental restraints	1506
total no. of NOE restraints	1426
intraresidue ($i = j$)	449
sequential ($ i - j = 1$)	364
medium-range ($2 \leq i - j \leq 5$)	209
long-range ($ i - j > 5$)	404
no. of H-bond restraints	20
no. of dihedral angle restraints (TALOS)	60
average non-intraresidue NOE's per residue	11.4
no. of NOE violations $> 0.3 \text{ \AA}$	0
no. of dihedral angle violations $> 5^\circ$	0
$\phi - \psi$ Space (residues ^[i, ii])	
most favored regions (%)	68.1
additionally allowed regions (%)	21.3
generously allowed regions (%)	10
disallowed regions (%)	0.7
rmsd's ^[iii, iv]	
backbone \AA	0.45 ± 0.09
heavy atoms \AA	1.38 ± 0.16

i. Residues considered: 11-95.

ii. From PROCHECK-NMR¹⁴

iii. Residues considered: 11-17, 25-29, 40-45, 62-66, 69-71, 90-95.

iv. Calculated using MOLMOL¹⁵.

The final ensemble (Figure 3.13) has backbone and side chain heavy atom rms deviations (rmsd) of $0.45 \pm 0.09 \text{ \AA}$ and $1.38 \pm 0.16 \text{ \AA}$, respectively for the well structured region. A PROCHECK-NMR¹⁴ analysis for the well structure region of the protein (residues 11-95) showed that 68.1% of the residues lie in the most favored region and 21.3% of the residues lie in the additionally allowed regions of the Ramachandran plot. 10% of the residues were observed in the generously allowed regions of the Ramachandran plot, while only 0.7% of the residues were found to be present in the disallowed region (figure 3.14). The structure was deposited in the PDB under accession code 1XZ9.

Figure 3.15a shows the experimental NOE restraints across the entire sequence of the protein. A lack of NOE restraints is apparent for residues K31-G39, which is reflected by increased backbone rms deviations in (Figure 3.15b) and a partially flexible loop region in the structural ensemble (Figure 3.13). The 'N' and 'C' termini are totally unstructured because no long range NOE's were observed.

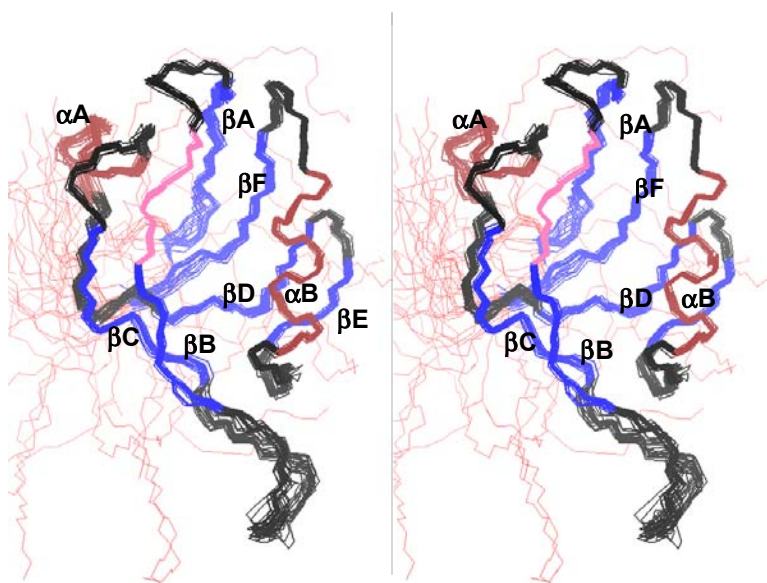


Figure 3.13: Solution NMR structure of AF6 PDZ domain: Superposition of the backbone (N, CA, and C') atoms for the 20 lowest-energy structures (stereo view). Color coding: α -helix-Brown (α A: 51-55, α B: 77-86), β -strands-Blue(β A:11-17, β B:25-29, β C:40-45, β D:62-66, β E:69-71, β F:90-95), loops-Black and the conserved GMGL loop-Pink (22-25)

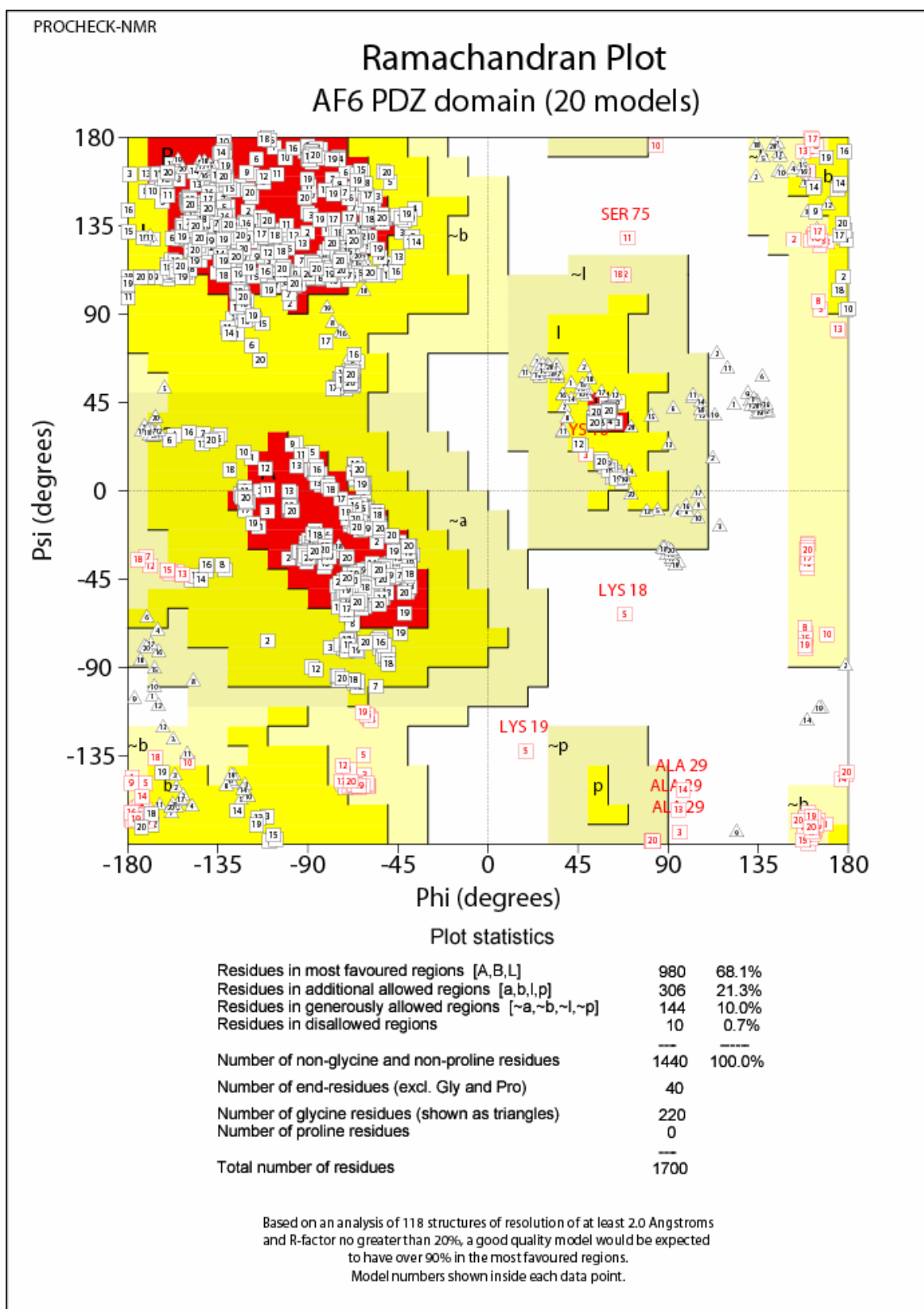


Figure 3.14: Ramachandran plot for the backbone ϕ and ψ angles of the AF6 PDZ domain. Procheck-NMR standard output

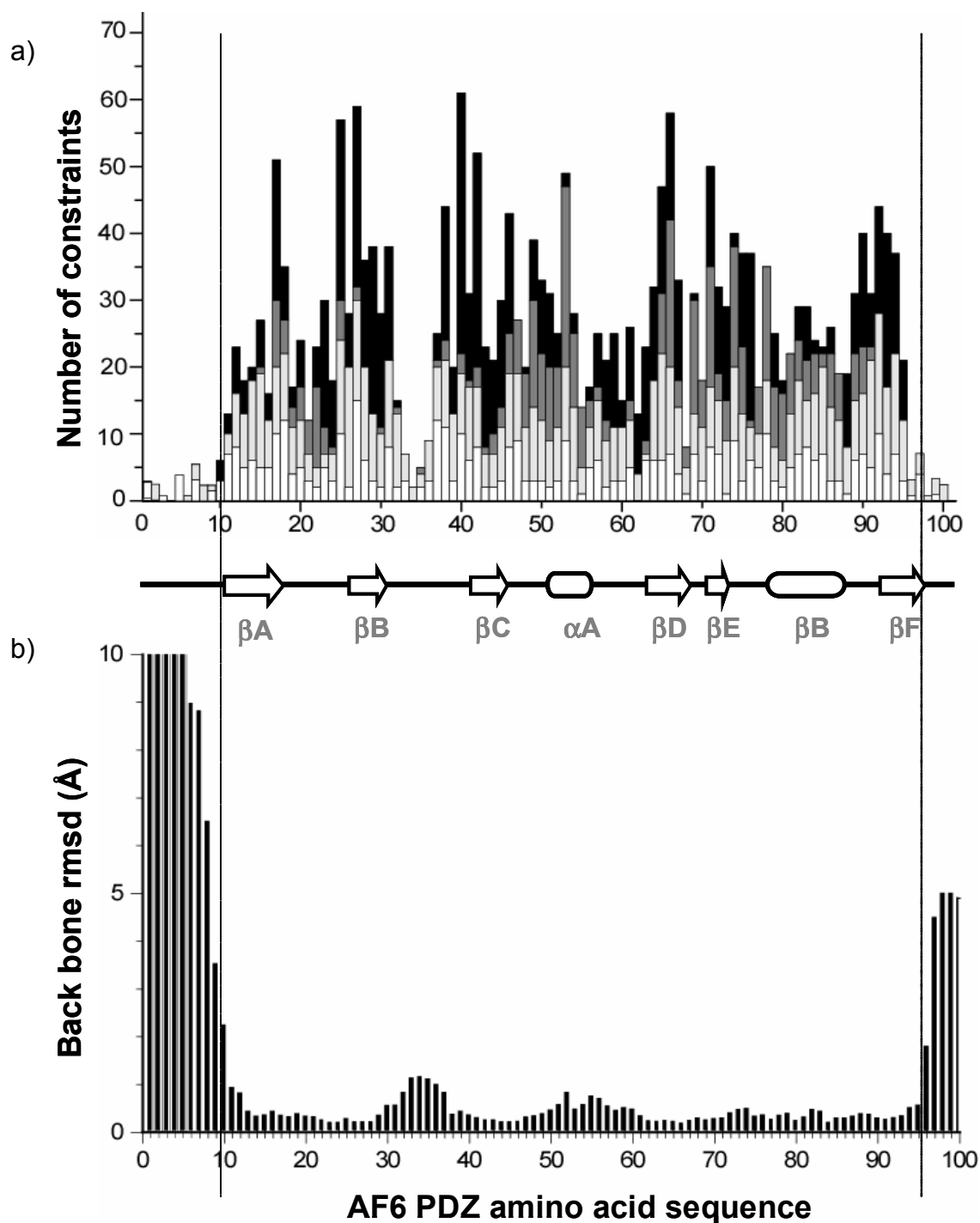


Figure 3.15: a) Distribution of short (white), medium-range (grey) and long-range (black) distance constraints across the AF6 PDZ domain. The figure was generated using the seqplot module of the program CYANA. b) RMSD plot for the backbone atoms of the AF6 PDZ domain ensemble. The figure shows the unstructured βB - βC loop, the N and the C terminus of the protein are also unstructured.

3.4.6 Structural Analysis

The AF6 PDZ domain structure is similar to other PDZ domains whose structure has been determined by X-ray crystallography and NMR.¹⁶⁻¹⁸ The secondary structure elements consist of six anti-parallel β -strands (β A- β F) and two α -helices (α A and α B) (Figure 3.16). Like many other modular protein interaction domains the 'N' and the 'C' termini of the AF6 PDZ domain are close to each other in the 3D structure.

Surface representation of the protein is shown in figure 3.17a and 3.17b. AF6 PDZ domain shows a well defined hydrophobic groove formed between β B and α B secondary structural elements which serves as the ligand binding pocket.

The signature "GLGF" carboxyl binding loop of other PDZ domains is replaced by a "GMGL" loop in the AF6 PDZ domain. Although the sequences are different, the hydrophobic side chains of Met23 and Leu25 point towards the interior of the protein forming a hydrophobic pocket which is recognized by the peptide 0 residue. (C-terminus of the ligand is designated as 0 and the preceding residues towards the N-terminus are number as -1, -2 ...)

Traditionally, AF6 PDZ domain was classified as Class II but it can also interact with Class I ligands.⁶ Closer inspection of the AF6 PDZ ligand binding groove reveals a glutamine residue (Glu76) at the α B1 position (first residue in α B helix). In canonical PDZ domain interactions, specificity is determined by the interaction between the α B1 residue and the -2 residue of the ligand.¹⁹ In Class II PDZ domains hydrophobic interaction between the α B1 and -2 ligand residue render specificity. In AF6 PDZ domain the Gln76 side chain, points towards the peptide binding groove, (Figure 3.18a and 3.18b) which renders unique characteristics to this pocket. Therefore it can be deduced that AF6 PDZ domain may interact with its ligands by a different mechanism than the canonical binding mode.

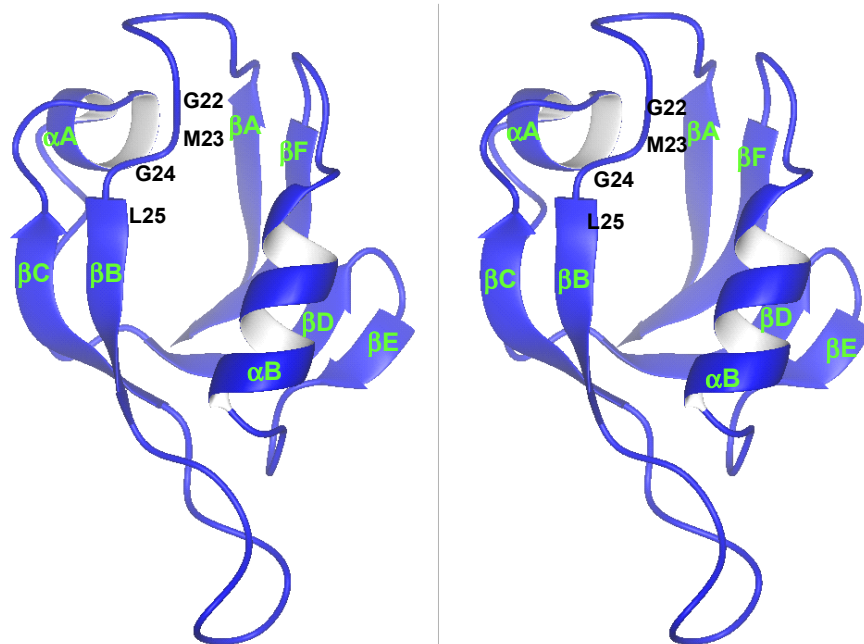


Figure 3.16: Ribbon representation of the AF6 PDZ domain structure as determined by CYANA. Only residues 11-95 shown.

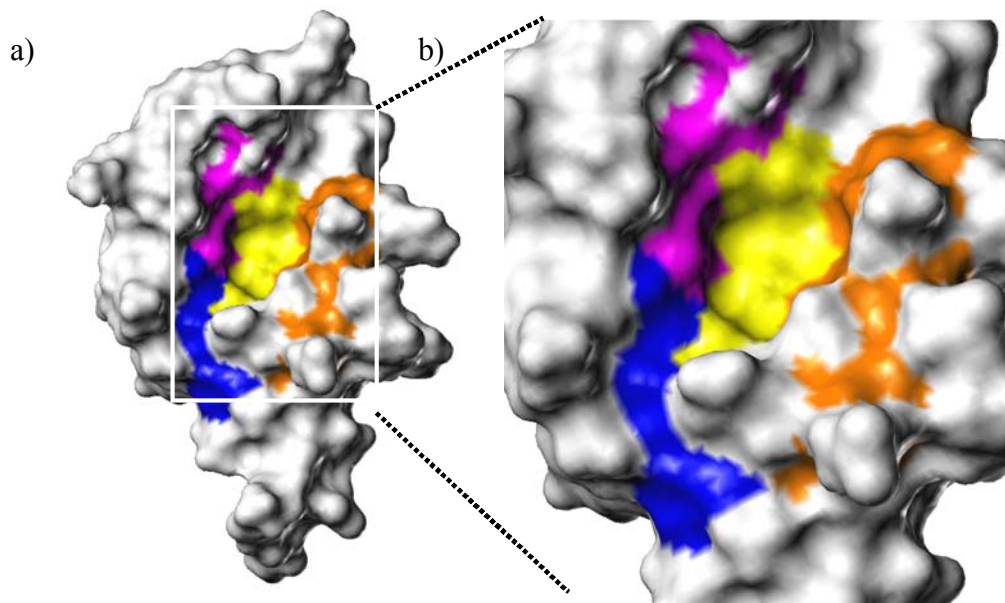


Figure 3.17: Surface representation of the AF6 PDZ domain. a) Overall topology of the AF6 PDZ domain. b) Closeup of the ligand binding groove. Color coding: Pink - Backbone of the residues in the GMGL loop, Blue - Backbone of the residues in β B and Orange - Backbone of the residues in α B.

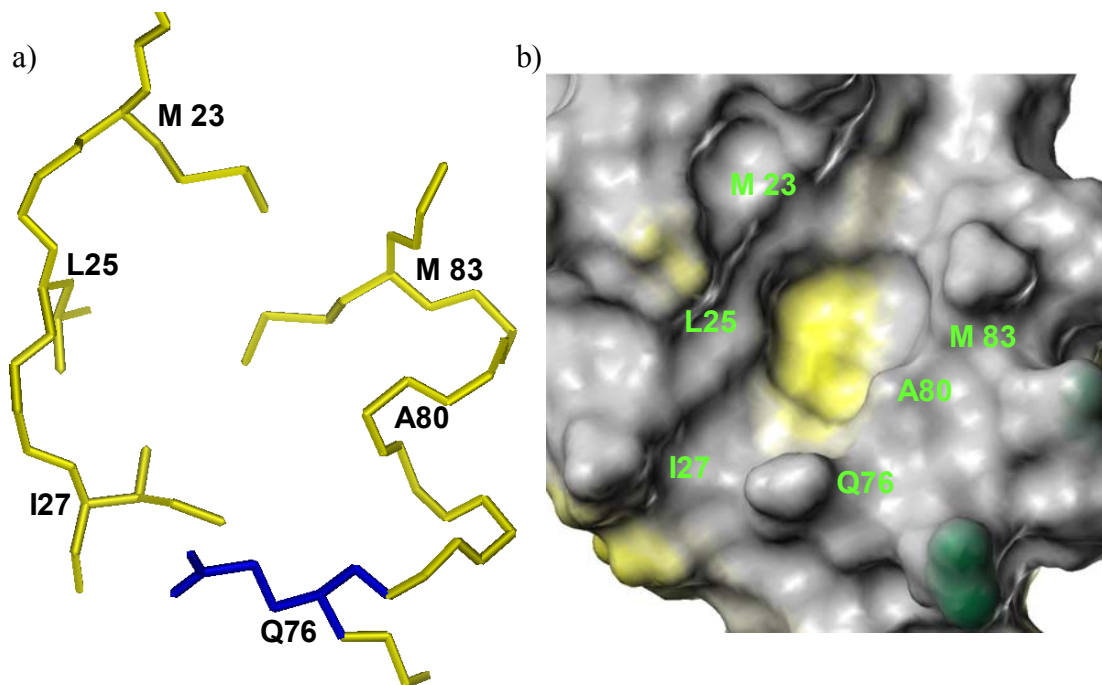


Figure 3.18: Binding cavity of the AF6 PDZ domain. a) Side chain orientations of the residues surrounding the binding cavity. The unique orientation of Gln76 is highlighted in blue. Only heavy atoms shown for clarity. b) Surface properties of the binding cavity. Color coding shows, yellow – hydrophobic regions and green – hydrophilic regions.

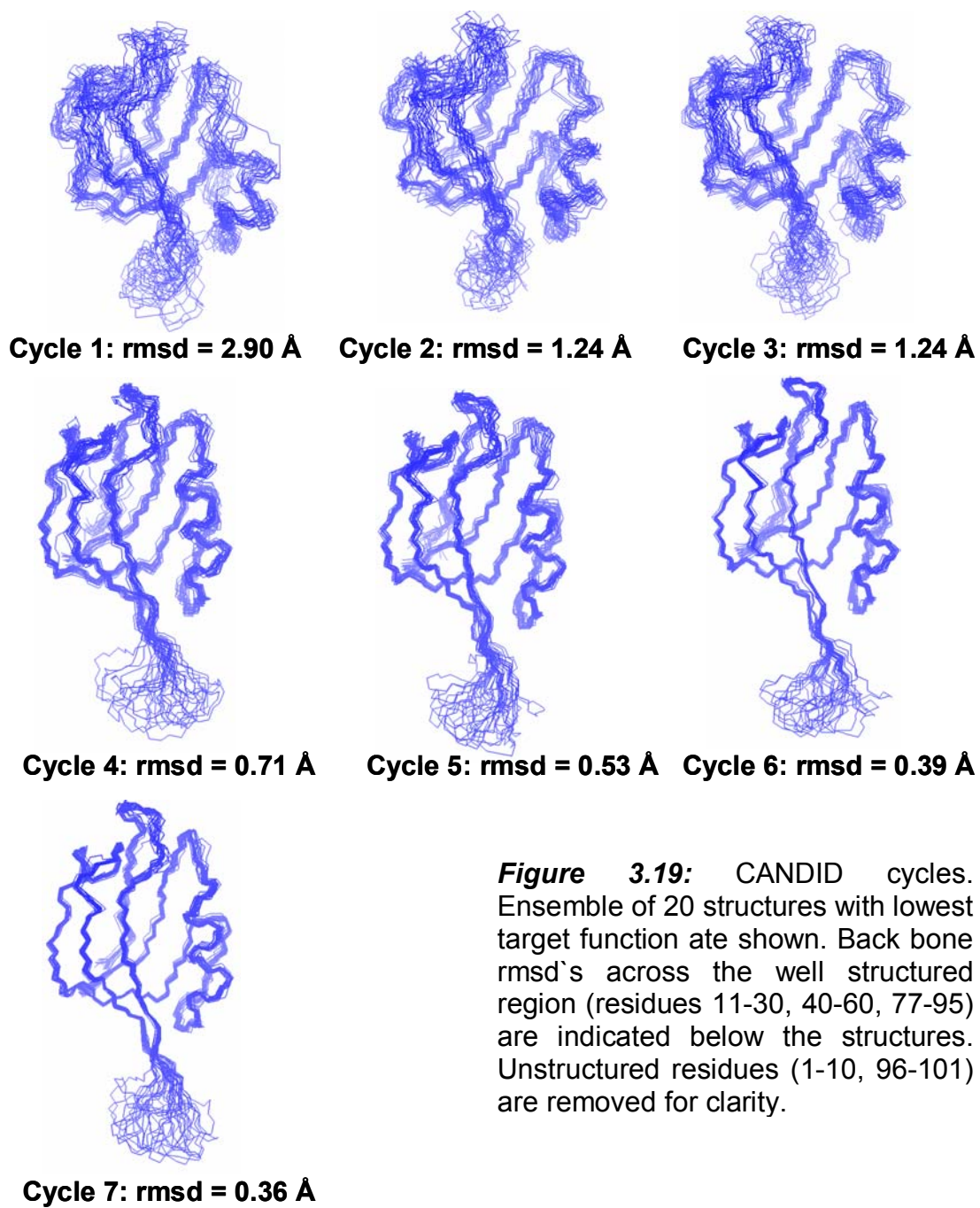
3.4.7 Structure determination of the AF6 PDZ - 5-(4-trifluoromethylbenzyl)-2-thioxo-4- thiazolidinone (7i) complex

To identify the protein-ligand interaction at atomic resolution, we determined the structure of the AF6 PDZ domain in complex with **7i**.

The structure determination process was essentially identical to that of the AF6 PDZ domain in the ligand-free form. All side-chain and NOE assignment spectra were recorded as described earlier on a sample containing AF6 PDZ domain and **7i** (1.5mM each).

The CANDID module of CYANA was used for the structure determination process. For this purpose a total of 1449 NOE derived distance restraints were used. In addition 64 dihedral angles from TALOS and 14 H-bond restraints based on the NOE pattern in the NOESY spectra were used. Chemical shift tolerances for the automated NOE assignments were kept at 0.02 ppm for the proton dimension and 0.3 ppm for the $^{13}\text{C}/^{15}\text{N}$ dimensions. Starting from a random coil orientation, 200 structures were calculated in each CANDID cycle. 20 structures having the lowest target function were accepted in the final ensemble. The convergence of the structures during subsequent CANDID cycles is illustrated in Figure 3.19.

Structural statistics for the final ensemble are listed in Table 3.6. Of the 1449 NOE derived distance restraints, 476 were long-range distance restraints ($|i - j| > 4$) which define the global fold of the protein. No distance restraint violations $> 0.3 \text{ \AA}$ and no angle restraint violations $> 5^\circ$ were observed. The final ensemble (figure 3.20) shows the backbone rms deviation (rmsd) of $0.48 \pm 0.09 \text{ \AA}$ and $1.21 \pm 0.23 \text{ \AA}$ for all the side chain heavy atoms. A PROCHECK-NMR analysis for the well structure region of the protein (residues 11-95) showed that 70.7% of the residues lie in the most favored region and 22.0% of the residues lie in the additionally allowed regions of the Ramachandran plot. Only 6.3 % and 0.7 % of the residues were found to be in the generously allowed and disallowed regions of the Ramachandran plot respectively (Figure 3.21). The structure was deposited in the PDB under accession code 2EXG.



Restrains	
total no. of experimental restraints	1527
total no. of NOE restraints	1449
intraresidue ($i = j$)	428
sequential ($ i - j = 1$)	390
medium-range ($2 \leq i - j \leq 5$)	155
long-range ($ i - j > 5$)	476
no. of H-bond restraints	14
no. of dihedral angle restraints (TALOS)	64
average nonintraresidue NOE's per residue	12
no. of NOE violations $> 0.3 \text{ \AA}$	0
no. of dihedral angle violations $> 5^\circ$	0
$\varphi - \psi$ Space (residues ^[i, iii])	
most favored regions (%)	70.7
additionally allowed regions (%)	22.0
generously allowed regions (%)	6.3
disallowed regions (%)	1.0
rmsd's ^[iii, iv]	
backbone \AA	0.48 ± 0.09
heavy atoms \AA	1.21 ± 0.23

Table 3.6: Structural statistics for the AF6 PDZ domain in complex with **7i**.

i. Residues considered: 11-95.

ii. From PROCHECK-NMR¹⁴

iii. Residues considered: 11-17, 25-29, 40-45, 62-66, 69-72, 77-95.

iv. Calculated using MOLMOL¹⁵.

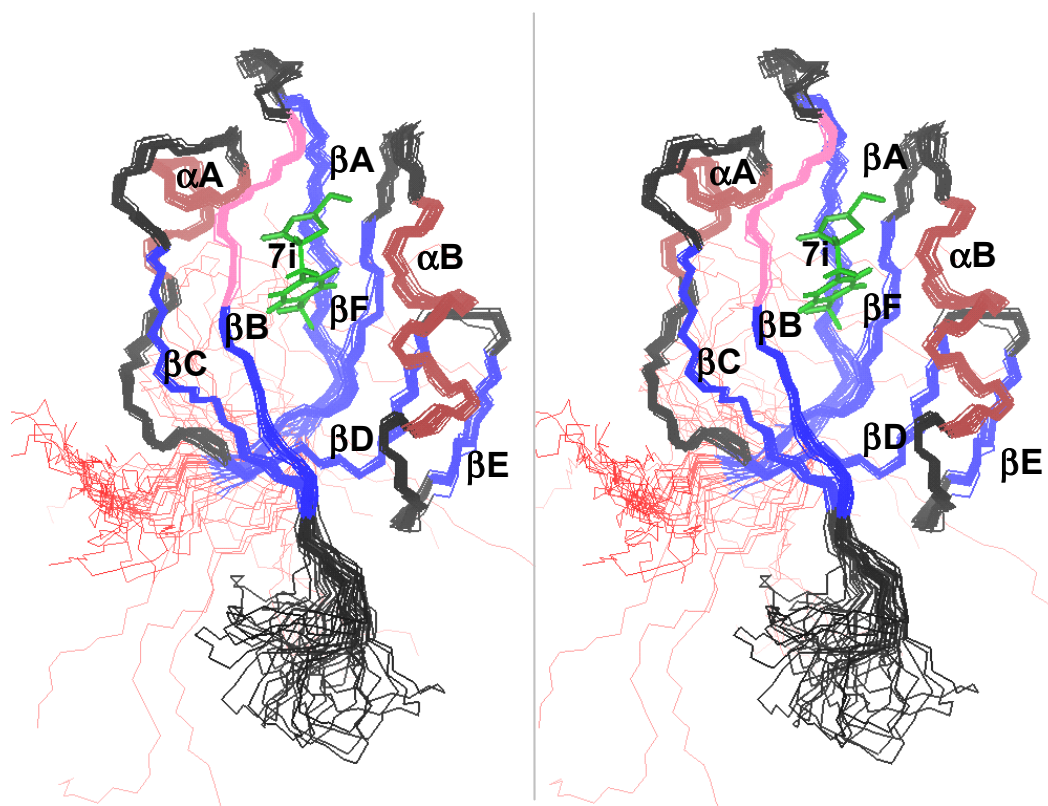


Figure 3.20: Solution NMR structure of AF6 PDZ domain in complex with 7i: Superposition of the backbone (N, CA, and C') atoms for the 20 lowest-energy structures (stereo view). Color coding: α -helix, brown (α A: 51-55, α B: 77-86); β -strands, blue (β A: 11-17, β B: 25-29, β C: 40-45, β D: 62-66, β E: 69-71, β F: 90-95); loops, black; conserved GMGL loop, pink (22-25)

Similar to the AF6 PDZ domain in the ligand-free form, the ligand-bound form shows distinct unstructured region between residues Lys31-Gly39. Analysis of the distance restraints show few or no long-range distance restraints for this region. (Figure 3.22a and 3.22b). No long-range restraints were observed for the unstructured 'N' and 'C' termini of the protein.

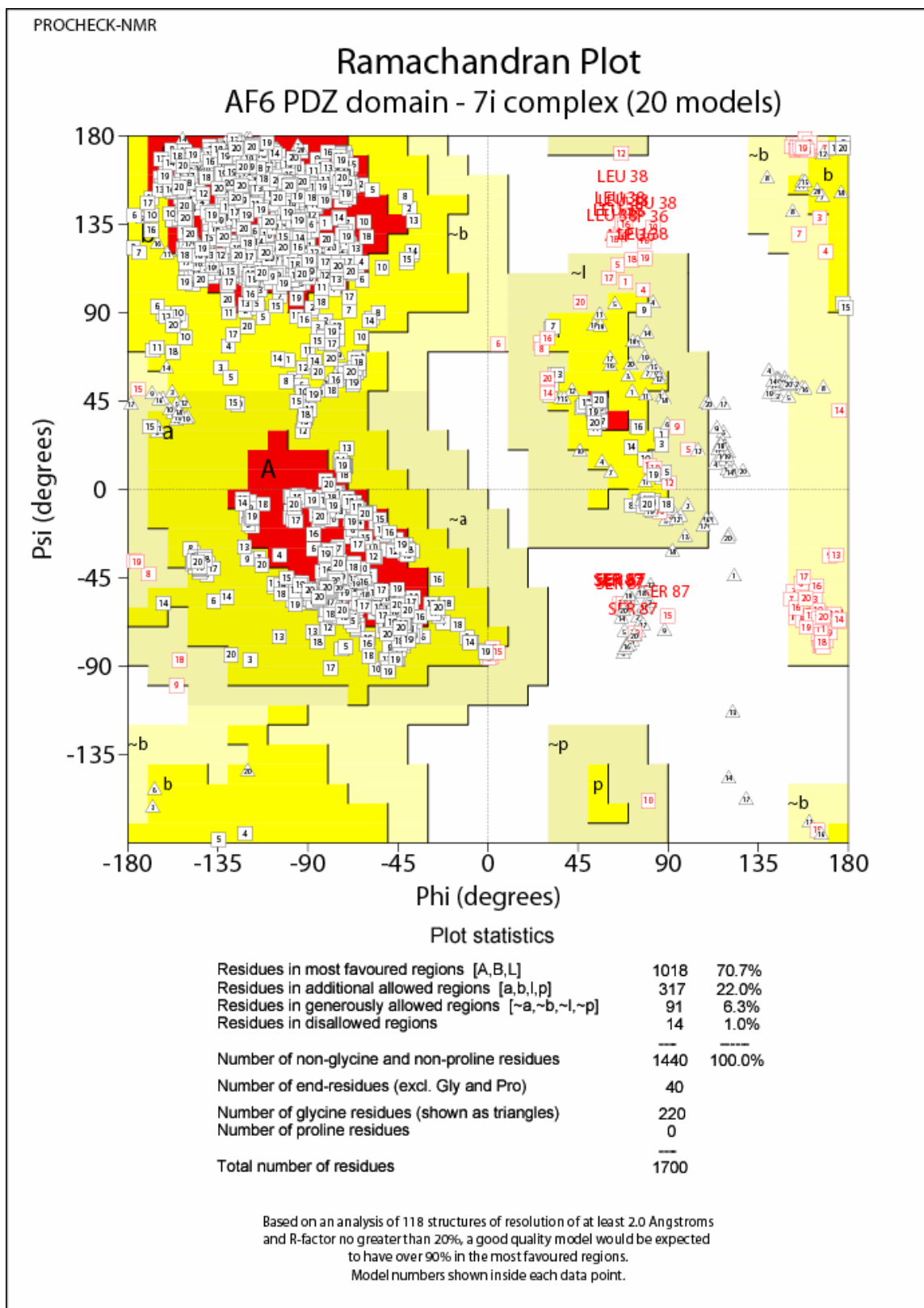


Figure 3.21: Ramachandran plot for the backbone ϕ and ψ angles of the AF6 PDZ domain. Procheck-NMR standard output

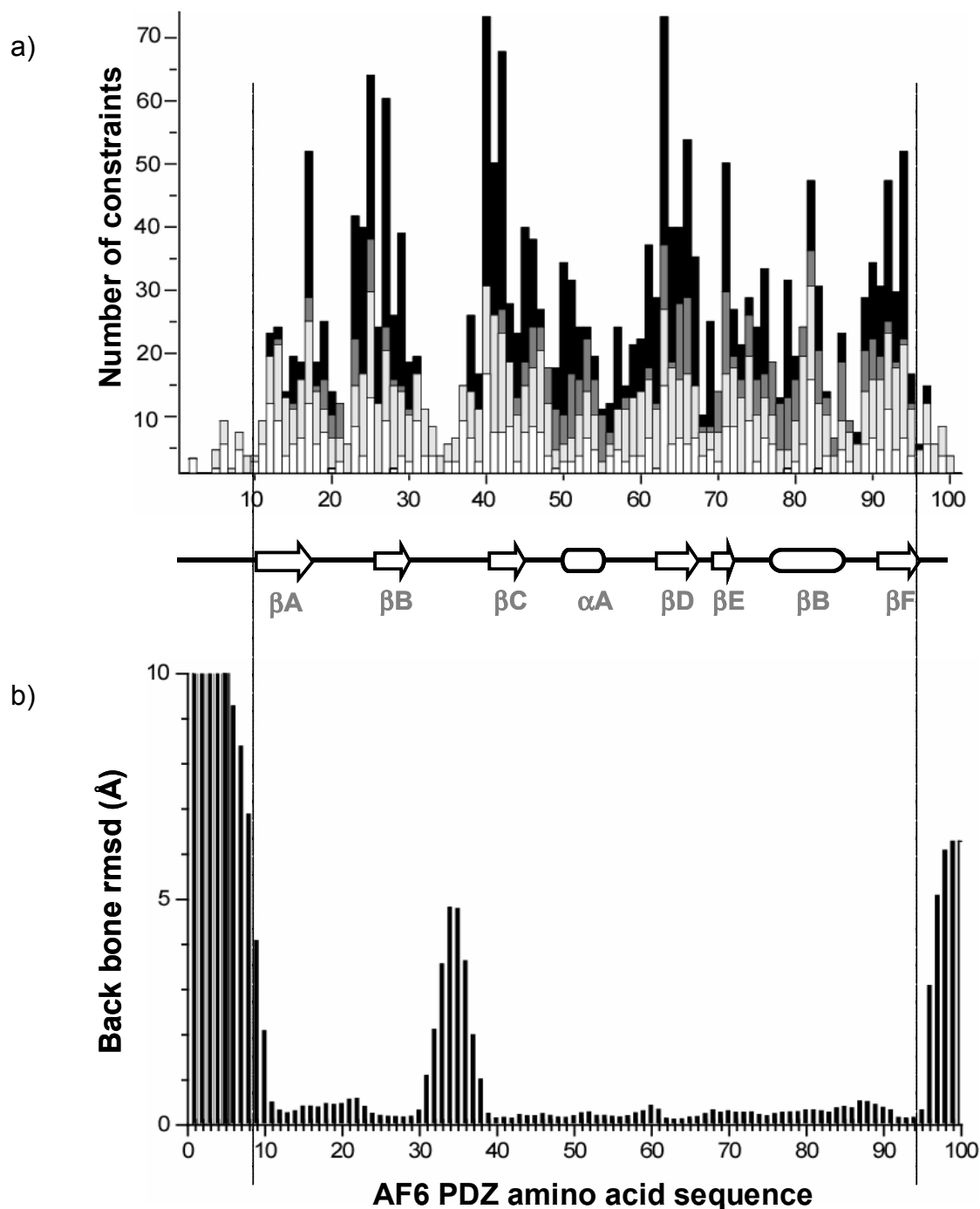


Figure 3.22: a) Distribution of short (white), medium-range (grey) and long-range (black) distance constraints across the AF6 PDZ domain. The figure was generated using seqplot module of the program CYANA. b) RMSD plot for the backbone atoms of the AF6 PDZ domain ensemble. The figure shows the unstructured βB - βC loop, the N and the C terminus of the protein are also unstructured.

Inter-molecular NOE's between the protein and **7i** were obtained from 2D ^{13}C -F2-filtered NOESY and 2D ^{13}C -F2-filtered HMQC-NOESY spectra. Because of the difference in the J couplings between ^1H - $^{13}\text{C}_{\text{ar}}$ and ^1H - $^{13}\text{C}_{\text{ali}}$ two spectra for each experiment were recorded (Aromatic filtered and aliphatic filtered). The C_5 -H signal overlaps with the water signal and was not observable even in the sample containing 100% D_2O . No intermolecular NOE's were observed for the C_6 - H_2 . A total of 11 intermolecular NOE's were extracted between the protein and the degenerate $\text{C}_{8/11}$ -H and $\text{C}_{9/10}$ -H atoms. The entire 11 NOE's occur between these degenerate protons and the side-chain protons of Met23, Leu25, Ile27, Ala80 Met83 and Thr84. (Figure 3.23a and 3.23b)

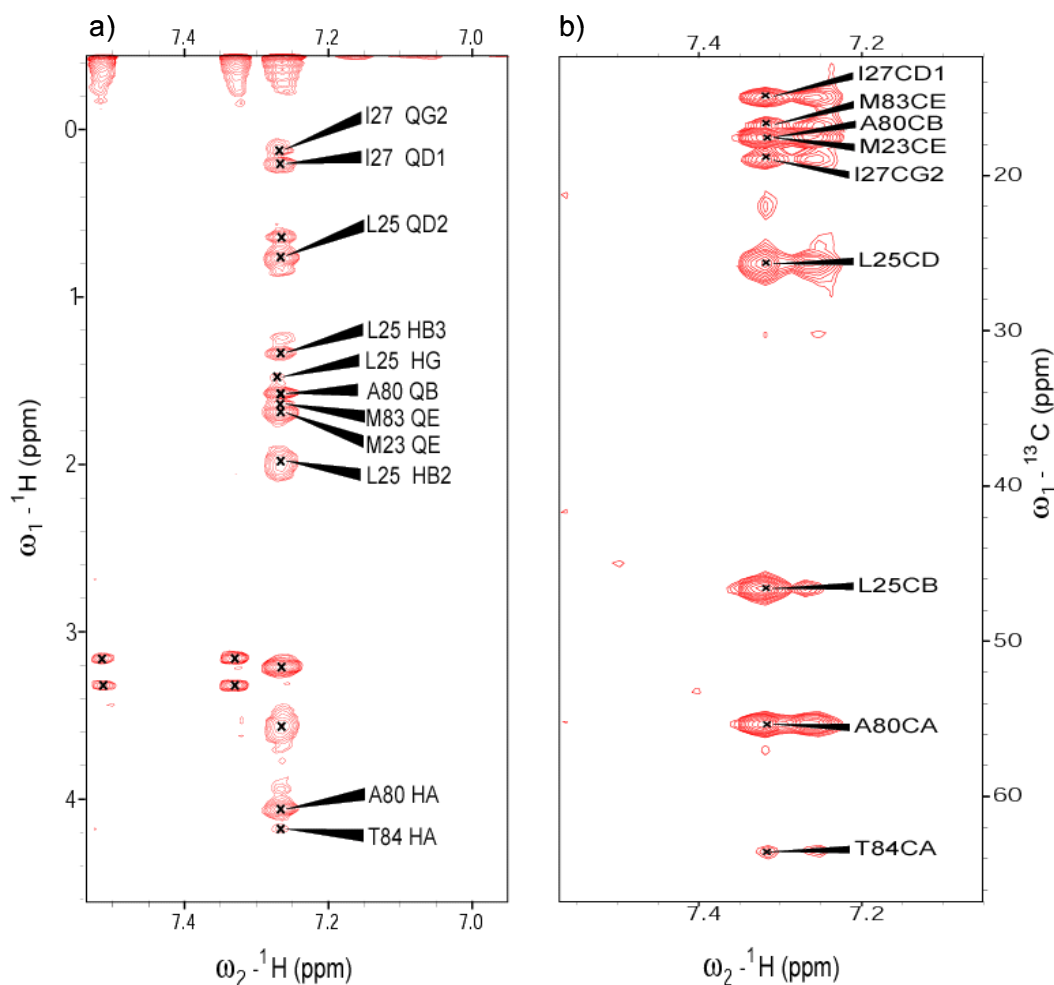


Figure 3.23: Spectra for inter-molecular NOEs between AF6 PDZ domain and **7i**. a) 2D-F2 ^{13}C -filtered NOESY. b) 2D-F2 ^{13}C -filtered HMQC-NOESY

No distance restraints were used to define the position of the thiazolidinone ring. Its position in a restrained molecular dynamics (MD) simulation was determined by the force field parameters of the docking program.

Following the assignment of the inter-molecular NOE's, both the R and the S enantiomers of **7i** were docked into the AF6 PDZ domain in the restrained MD. For the docking purpose the AF6 PDZ domain structure with lowest target function was used. Initially, **7i** was manually docked into the protein using the program Sybyl 6.91. The structure of the manually docked complex was then read into the program LEaP for preparation of the topology and coordinate files to be used in the MD run.

In the first step of the MD, the solvated complex was minimized to remove bad contacts. If a MD is carried out in the presence of bad contacts the energy for this region will become extremely high which may misguide the MD trajectory into an unrealistic direction. A short energy minimization run of 1000 steps was sufficient to relax the system.

The initial trajectories, in which solute and solvent undergo relaxation before reaching a stationary state, are generally discarded in MD simulations. This stage of the MD is called equilibration stage. For the AF6 PDZ **7i** complex, a 100 ps equilibration run was performed. In the first step of equilibration the temperature of the system was increased from 1 K to 300 K over 20 ps. Once the temperature had stabilized, the density of water was adjusted to the experimental values by applying pressure and temperature control. By the end of the equilibration step the system had stabilized at ~300K and the density of water was adjusted to ~1 gram/ml from a starting value of 0.56 gram/ml. (Figure 3.24)

Following the minimization and equilibration steps, **7i** was docked into the AF6 PDZ domain in a restrained MD simulation run lasting 2 ns in Amber8.²⁰ For the first 1.5 ns, the ligand was docked into the protein by using all 11 NOE restraints. During the final 0.5 ns the distance restraints were gradually removed to check the viability of the docking process.

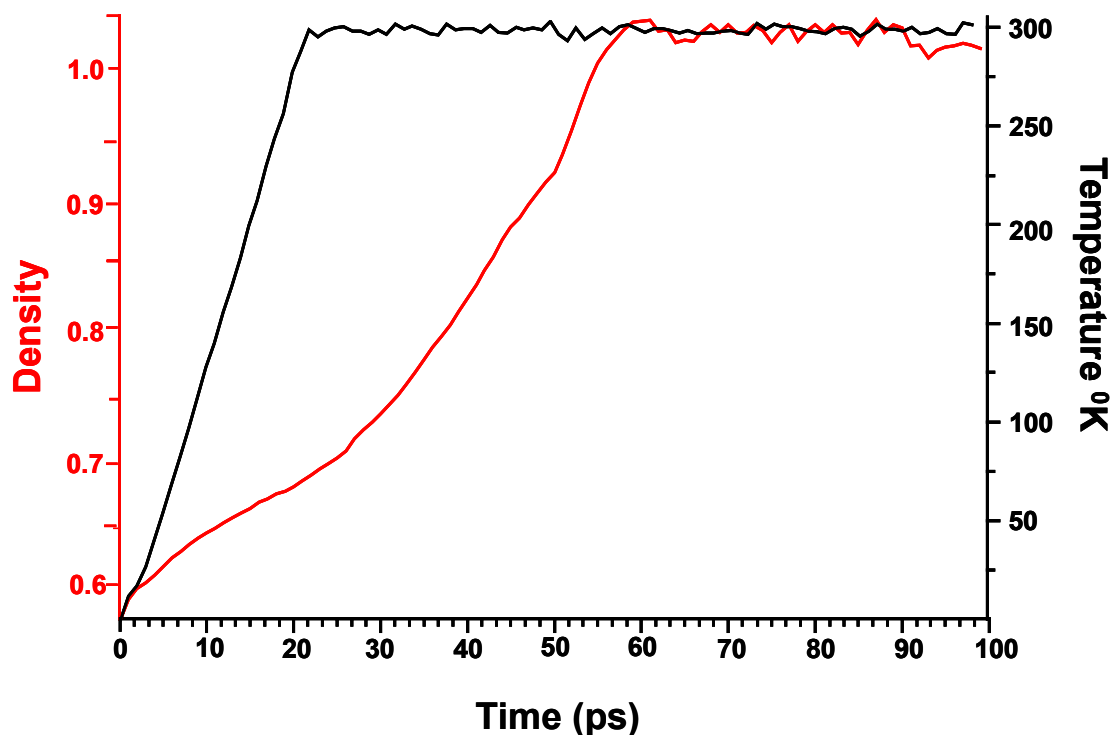


Figure 3.24: Stabilization of the temperature (Black line) and equilibration of the density of water to experimental conditions (~1gram/ml) (Red line) during the initial MD steps.

While the potential energy curves of both enantiomers decrease, the total potential energy for the S enantiomer (-3100 kcal/mol) is significantly higher than that of the R enantiomer (-3790 kcal/mol). Therefore it can be safely assumed that the R enantiomer is most likely the preferred ligand of the AF6 PDZ domain.

3.4.8 Structural analysis of the AF6 PDZ - 5-(4-trifluoromethylbenzyl)-2-thioxo-4-thiazolidinone (**7i**) complex

AF6 PDZ domain in complex with **7i** shows the same fold as the ligand-free protein. Figure 3.25 shows the structure of the AF6 PDZ domain in complex with **7i**. **7i** binds to the AF6 PDZ in the ligand binding groove.

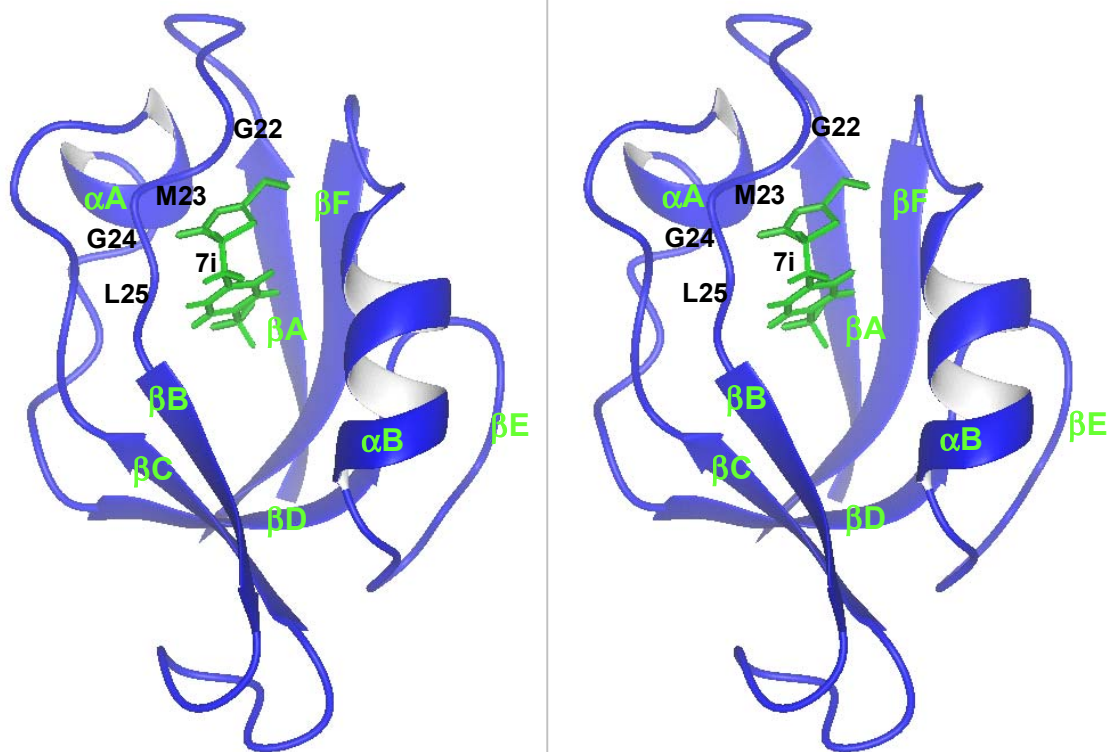
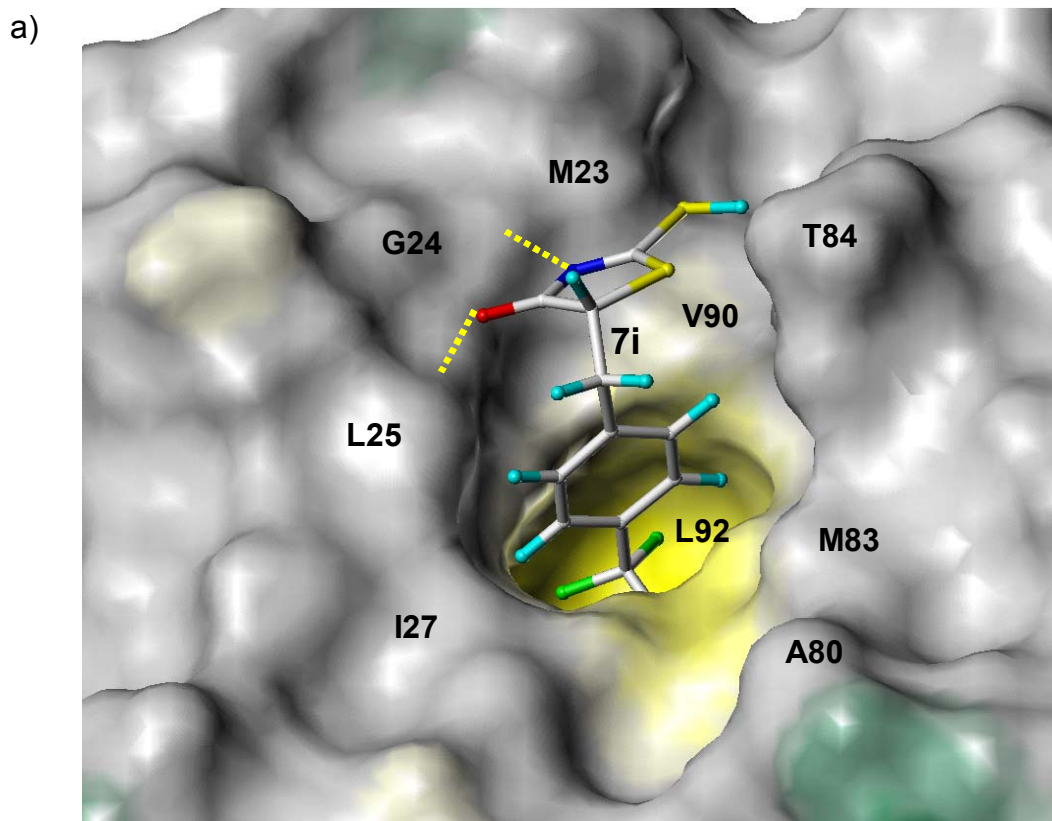


Figure 3.25: Ribbon representation of the AF6 PDZ - **7i** complex structure as determined by CYANA. Only residues 11-95 shown. The docked ligand is colored green.

Analysis of the protein surface shows the presence of a deep hydrophobic pocket in the vicinity of the “GMGL” loop. The pocket is surrounded by the side chains of the residues Met23, Leu25, Ile27, Ala80, Met83 and Leu92. This pocket is absent in the structure of the ligand-free protein suggesting significant side-chain rearrangement of the residues in the binding groove. The CF₃-Ph group of **7i** is embedded in this hydrophobic pocket while N3 and O4 of the ligand form H-bonds with the backbone HN’s of residues Gly24 and Leu25 (Figure 3.26a, 3.26b and 3.26c). This binding mode is in agreement with the importance of an

unsubstituted N3 in the five membered ring and also explains the significantly lower affinity of other analogues.

The lower affinity of compounds **7a**, **7b**, **7c** and **7f** as compared to **7i** can be explained by the sub-optimal occupancy of the hydrophobic pocket. The weak binding of **7k** can be attributed to steric hindrance because the m-CF₃ substituted phenyl ring would require a larger hydrophobic pocket. A combination of steric effect and unfavorable interactions might be the reason behind the inactivity of **7g**.



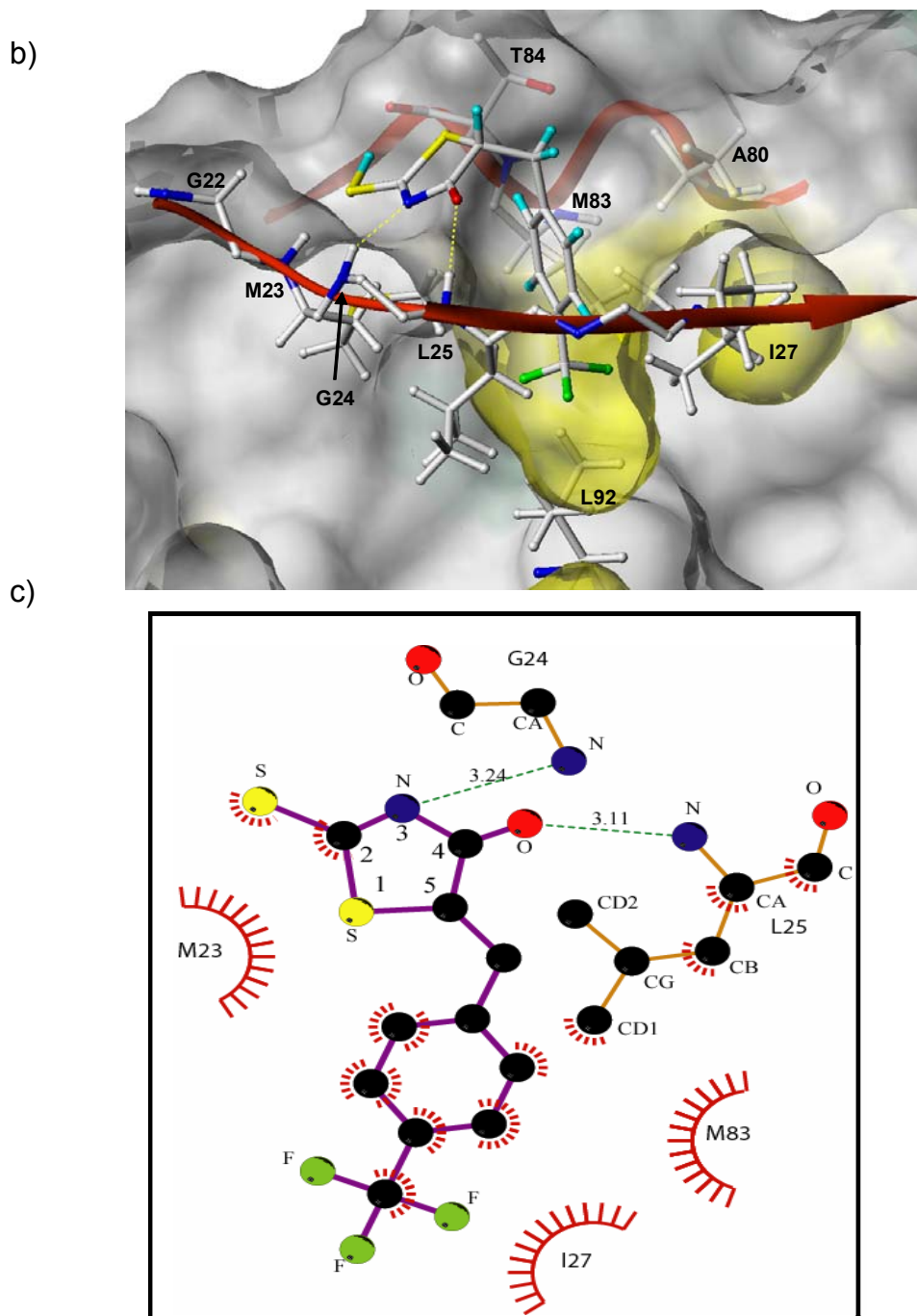


Figure 3.26: AF6 PDZ domain in complex with 7i. a) Top view, b) Lateral view. Surface coloring indicated hydrophobic (yellow) and hydrophilic (green) areas. Hydrogen bonds between AF6 PDZ and 7i are indicated by yellow dotted lines. c) Schematic representation of the AF6 PDZ – 7i interaction. Hydrogen bonds are shown as green dotted lines. Hydrophobic interactions are highlighted by red line fences. The figure was generated using the program Ligplot.²¹

3.5 Comparison of the ligand-free and ligand-bound AF6 PDZ domain:

To better understand the mode of binding of **7i** to the AF6 PDZ domain, we compared the structures of AF6 PDZ in the ligand-free and ligand-bound form. The superposition between the ligand-free and ligand-bound AF6 PDZ shows an α -carbon rmsd of 1.25 Å when the structurally conserved β strands are used for the superposition. Three areas of significant differences were observed in the two structures: α -helices α A and β B and β -strand β E. (Figure 3.27a) The significance of the deviation of α A is unclear because it has no known function in PDZ domain interactions. The shift in α B helix is functionally more significant as it forms the ligand binding groove along with β B. The binding of **7i** to the protein causes a shift of 3.3 Å in the C α atom of Gln76 at the beginning of α B which resulted in the widening of the peptide binding groove.

Closer inspection of the superimposed structures reveals significant side-chain rearrangement of the hydrophobic amino acids in the ligand binding groove. The side chains of Met23, Leu25, Ala80 and Met83 are rearranged to accommodate the bulky CF₃-Ph group of **7i** (Figure 3.27b). The side chains of the other hydrophobic residues lining this pocket (Ile27 and Leu92) show very little side-chain rearrangement (Figure 3.27b). These observations suggest that the 3.3 Å shift at the beginning of α B is a result of the movement of the side-chains of residues Ala80 and Met83 which are pushed away from β B to give room for **7i**. The shifting of the β E-strand is likely to be a direct consequence of the shifting of the α B-helix.

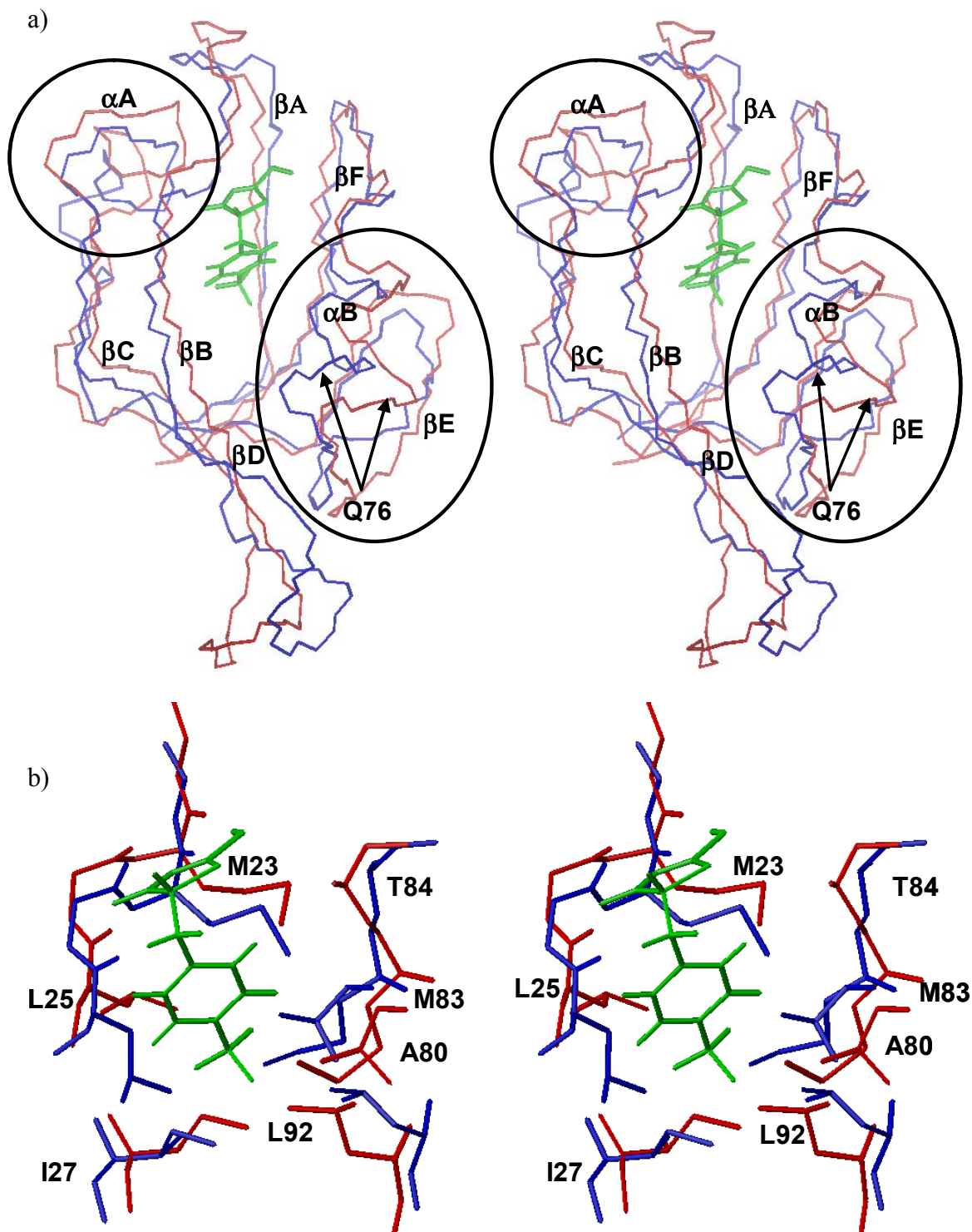


Figure 3.27: a) comparison of AF6 PDZ domain in ligand-free (blue) and ligand-bound (red) form. **7i** is colored green (stereoview). The areas of significant difference are highlighted. b) Side chain rearrangement of the residues in the binding groove (stereoview).

3.6 Comparison of the ligand-bound AF6 PDZ domain to the syntrophin and erbin PDZ domains

At this early stage in the ligand development process, we expected **7i** to be unspecific towards the PDZ domain sub-classes. To get insight into the possible interaction of **7i** with other classes of PDZ domains, we compared the structure of AF6 PDZ in the ligand-bound form to the crystal structures of the syntrophin (1QAV)¹ and erbin (1MFG)² PDZ domains in complex with their respective peptide ligands. AF6 PDZ in the ligand-bound form superimposes well with these two PDZ domains with rmds of 1.7 and 1.5 Å, respectively.

In the structure of syntrophin PDZ all residues homologous to the **7i** contacting residues of AF6 PDZ, adopt similar positions. Only Leu149 needs to undergo a slight side-chain rearrangement to make sufficient space to accommodate the CF₃-Ph group of **7i**, (Figure 3.28a) suggesting that **7i** may interact similarly with syntrophin PDZ. Our experimental data on **7i** binding to syntrophin PDZ (Figure 3.28b) show similar CSPs as observed for AF6 PDZ, supporting the structure-based prediction of an akin interaction mode.

In syntrophin PDZ a histidine is present at the beginning of α B. The homologous position is occupied by a glutamine in the AF6 PDZ domain. These two residues overlay with each other in the two structures, suggesting that the variation of **7i** specifically designed to interact with these residues, would be helpful in developing specific ligands.

In the structure of erbin PDZ the bulky side-chain of Phe1293, which is homologous to Leu25 of AF6 PDZ, severely clashes with the CF₃ moiety of **7i** (Figure 3.29). As the conformational freedom of the Phe1293 side-chain is limited, binding specificity to AF6 PDZ-like versus erbin PDZ-like domains may be controlled by such CF₃ or related moieties. Other residues including the

homologues of Ile27 and Ala80 which play an important role for the recognition of hydrophobic -2 position residues of cognate peptides, show similar orientations.

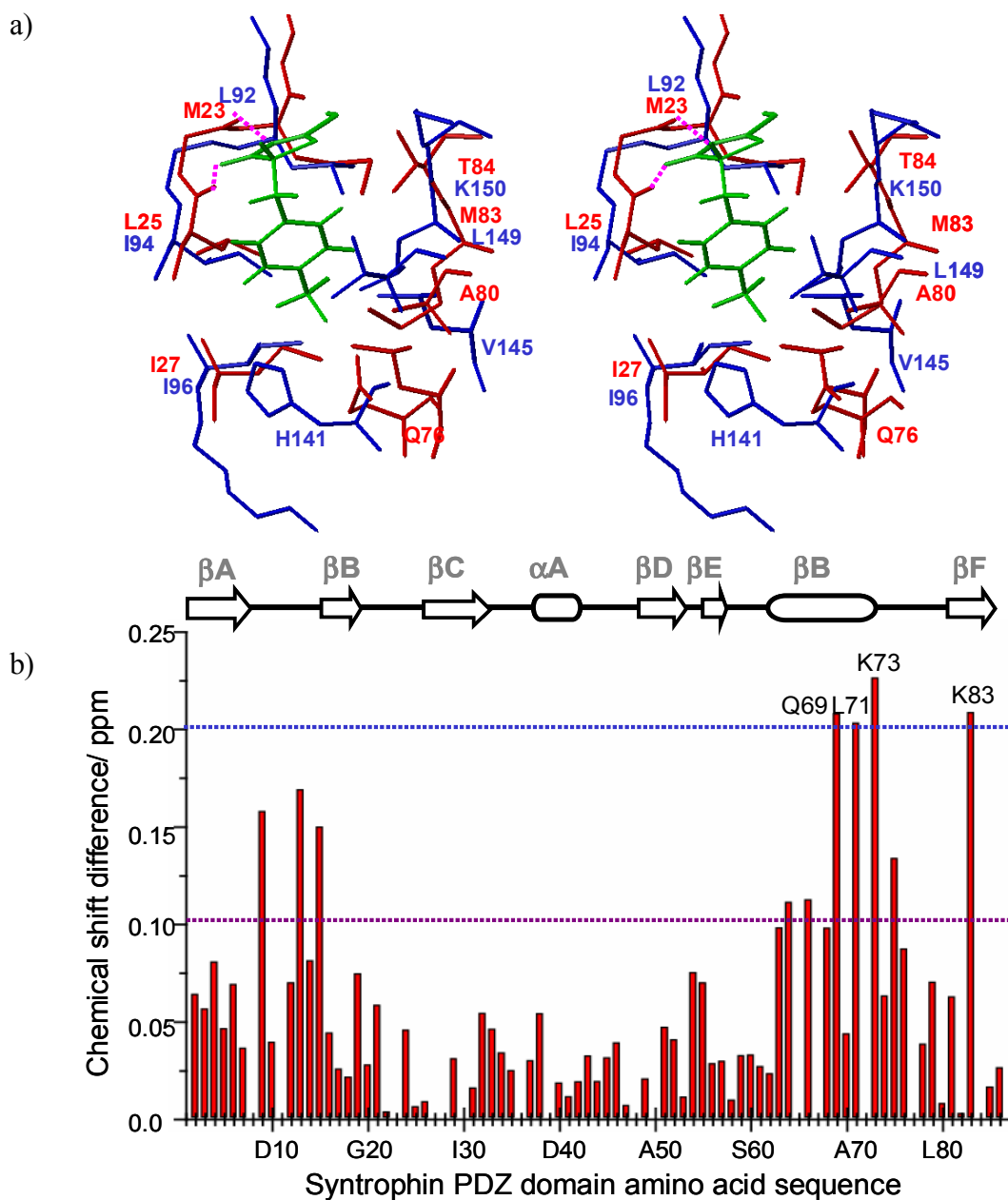


Figure 3.28: a) Comparison of AF6 PDZ ligand-bound (red) state and syntrophin PDZ domain bound to nNOS β -finger (PDB code 1QAV) (blue) (stereoview). b) CSPs of the backbone HN's of the syntrophin PDZ domain in presence of **7i**

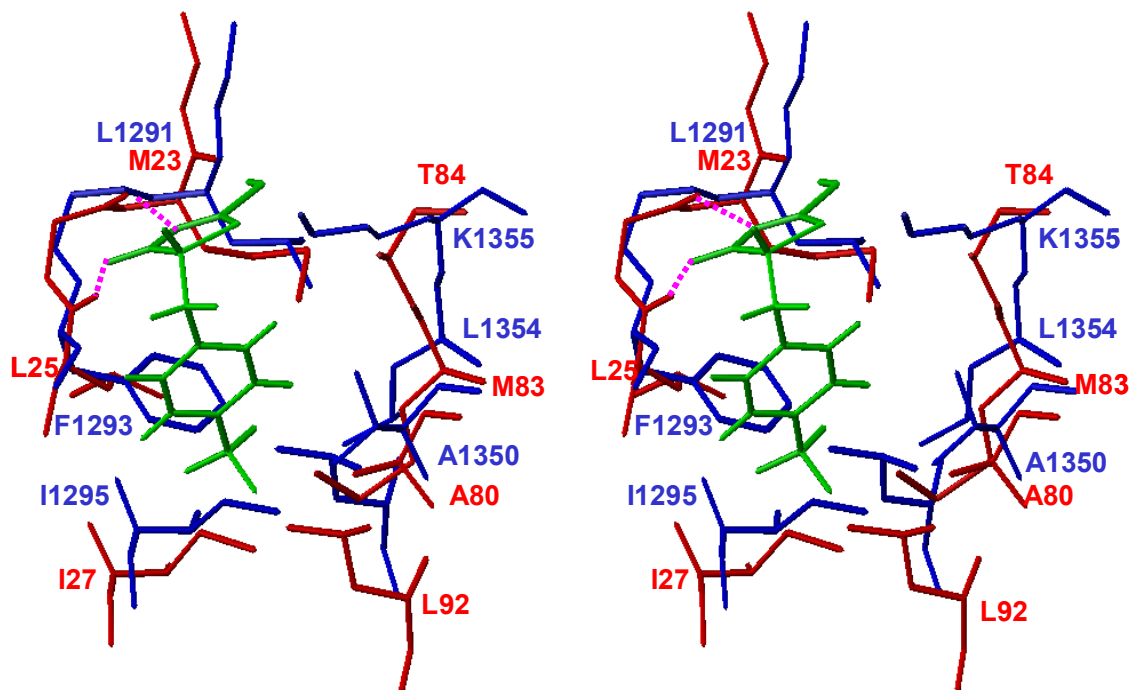


Figure 3.29: Comparison of AF6 PDZ ligand-bound (red) state and erbin PDZ domain bound to Erbb2 receptor peptide (PDB code 1MFG) (blue) (stereoview).

These observations indicate that, although **7i** might be non-specific towards the PDZ domain sub-classes, subtle variation of this compound might lead to specific ligands.

3.7 References

- (1) Hock, B., B. Bohme, T. Karn, T. Yamamoto, K. Kaibuchi, U. Holtrich, S. Holland, T. Pawson, H. Rubsamen-Waigmann and K. Strebhardt PDZ-domain-mediated interaction of the Eph-related receptor tyrosine kinase EphB3 and the ras-binding protein AF6 depends on the kinase activity of the receptor. *Proc Natl Acad Sci U S A.* **1998**, *95*, 9779-9784.
- (2) Buchert, M., S. Schneider, V. Meskenaite, M.T. Adams, E. Canaani, T. Baechi, K. Moelling and C.M. Hovens. The junction-associated protein AF-6 interacts and clusters with specific Eph receptor tyrosine kinases at specialized sites of cell-cell contact in the brain. *J. Cell. Biol* **1999**, *144*, 361-371.
- (3) Takahashi, K., H. Nakanishi, M. Miyahara, K. Mandai, K. Satoh, A. Satoh, H. Nishioka, J. Aoki, A. Nomoto, A. Mizoguchi and Y. Takai. Nectin/PRR: an immunoglobulin-like cell adhesion molecule recruited to cadherin-based adherens junctions through interaction with Afadin, a PDZ domain-containing protein. *J. Cell. Biol* **1999**, *145*, 539-549.
- (4) Ebnet, K., C.U. Schulz, M.K. Meyer Zu Brickwedde, G.G. Pendl and D. Vestweber. Junctional adhesion molecule interacts with the PDZ domain-containing proteins AF-6 and ZO-1. *J. Biol. Chem* **2000**, *275*, 27979-27988.
- (5) Radziwill, G., R.A. Erdmann, U. Margelisch and K. Moelling. The Bcr kinase downregulates Ras signaling by phosphorylating AF-6 and binding to its PDZ domain. *Mol Cell Biol* **2003**, *23*, 4663-4672.
- (6) Wiedemann, U., P. Boisguerin, R. Leben, D. Leitner, G. Krause, K. Moelling, R. Volkmer-Engert and H. Oschkinat. Quantification of PDZ domain specificity, prediction of ligand affinity and rational design of super-binding peptides. *J. Mol. Biol.* **2004**, *343*, 703-718.
- (7) Lipinski, C. A., F. Lombardo, B.W. Dominy and P.J. Feeney. Experimental and computational approaches to estimate solubility and permeability in drug discovery and development settings. *Advanced Drug Delivery Reviews* **1997**, *23*, 3-25.
- (8) Bemis, G. W., and M.A. Murcko. The properties of known drugs. 1. Molecular Frameworks. *J. Med.Chem* **1996**, *39*, 2887-2893.
- (9) Bemis, G. W., and M.A. Murcko. The properties of known drugs 2. Side chains. *J. Med.Chem* **1996**, *42*, 5095-5099.
- (10) Goddard, T. D., D.G. Kneller. SPARKY 3. *University of California, San Francisco.* **2003**.
- (11) Wishart, D. S., B. D. Sykes and F. M. Richards The Chemical-Shift Index - a Fast and Simple Method for the Assignment of Protein Secondary Structure through Nmr-Spectroscopy. *Biochemistry* **1992**, *31*, 1647-1651.
- (12) Wishart, D. S., and B. D. Sykes The C-13 Chemical-Shift Index - a Simple Method for the Identification of Protein Secondary Structure Using C-13 Chemical-Shift Data. *J. Bio. Mol. NMR* **1994**, *4*, 171-180.
- (13) Herrmann, T., P. Guntert and K. Wuthrich Protein NMR structure determination with automated NOE assignment using the new software

-
- CANDID and the torsion angle dynamics algorithm DYANA. *Journal of Molecular Biology* **2002**, *319*, 209-227.
- (14) Laskowski, R. A., J. A. Rullmann, M. W. MacArthur, R. Kaptein and J. M. Thornton AQUA and PROCHECK-NMR: programs for checking the quality of protein structures solved by NMR. *J. Bio. Mol. NMR* **1996**, *8*, 477-486.
- (15) Koradi, R., M. Billeter and K. Wüthrich. MOLMOL: a program for display and analysis of macromolecular structures. *J Mol Graphics* **1996**, *14*, 51-55.
- (16) Schultz, J., U. Hoffmuller, G. Krause, J. Ashurst, M.J. Macias, P. Schmieder, J. Schneider-Mergener, H. Oschkinat Specific interactions between the syntrophin PDZ domain and voltagegated sodium channels. *Nature Struct. Biol.* **1998**, *5*, 19-24.
- (17) Stricker, N. L., K.S. Christopherson, B.A. Yi, P.J. Schatz, R.W. Raab, G. Dawes, D.E. Bassett Jr, D.S. Bredt, M. Li PDZ domain of neuronal nitric oxide synthase recognizes novel C-terminal peptide sequences. *Nature. Biotech.* **1997**, *15*, 336-342.
- (18) Doyle, D. A., A. Lee, J. Lewis, E. Kim, M. Sheng, R. MacKinnon Crystal structures of a complexed and peptide-free membrane protein- binding domain: molecular basis of peptide recognition by PDZ. *Cell* **1996**, *85*, 1067-1076.
- (19) Sonyang, Z., A.S. Fanning, C. Fu, J. Xu, S.M. Marfatia, A.H. Chishti, A. Crompton, A.C. Chan, J.M. Anderson and L.C. Cantley. Recognition of Unique Carboxyl-Terminal Motifs by Distinct PDZ Domains. *Science* **1997**, *275*, 73-77.
- (20) Case, D. A., T.A. Darden, T.E. Cheatham, III, C.L. Simmerling, J. Wang, R.E. Duke, R. Luo, K.M. Merz, B. Wang, D.A. Pearlman, M. Crowley, S. Brozell, V. Tsui, H. Gohlke, J. Mongan, V. Hornak, G. Cui, P. Beroza, C. Schafmeister, J.W. Caldwell, W.S. Ross, P.A. Kollman AMBER 8. *University of California, San Francisco.* **2004**.
- (21) Wallace, A. C., R.A. Laskowski and J.M. Thornton LIGPLOT: A program to generate schematic diagrams of protein-ligand interactions. *Prot. Eng.* **1995**, *8*, 127-134.
- (22) Hillier, B. J., K. S. Christopherson, K. E. Prehoda, D. S. Bredt and W. A. Lim Unexpected Modes Of PdZ Domain Scaffolding Revealed By Structure Of Nnos- Syntrophin Complex. *Science* **1999**, *284*, 812-815.
- (23) Birrane, G., J. Chung and J. A. Ladas Novel mode of ligand recognition by the Erbin PDZ domain. *J. Biol. Chem* **2003**, *278*, 1399-1402.
-